Geoscience Canada
Journal of the Geological Association of Canada
Journal de l'Association Géologique du Canada

Igneous Rock Associations 29. The Nenana Magnetitite Lava Flow, Alaska Range, Alaska

S.P. Reidel, M.E. Ross and J. Kasbohm

Volume 50, Number 2, 2023

URI: https://id.erudit.org/iderudit/1102302ar
DOI: https://doi.org/10.12789/geocanj.2023.50.197

See table of contents

Publisher(s)

The Geological Association of Canada

ISSN

0315-0941 (print)
1911-4850 (digital)

Explore this journal

Cite this article

Reidel, S., Ross, M. & Kasbohm, J. (2023). Igneous Rock Associations 29. The Nenana Magnetitite Lava Flow, Alaska Range, Alaska. *Geoscience Canada*, *50*(2), 53–71. https://doi.org/10.12789/geocanj.2023.50.197

Article abstract

Magnetitite deposits like El Laco (Chile) are rare and have controversial origins. An unusual magnetitite lava flow overlying a rhyolite unit occurs in the north-central Alaska Range and originally covered ~ 750 km2 of the Miocene Nenana basin. Dating of the rhyolite and relationships between the magnetitite and sedimentary rocks indicate that both are of Late Miocene age. The magnetitite flow is mainly magnetite with some post-eruptive alteration to hematite. Both the rhyolite flow and the magnetitite flow are vesicular, but the magnetitite flow also has small, millimetre-scale columnar jointing. The vesicular zones in the magnetitite flow grade into massive rock on the scale of a thin section, suggesting a degassing lava origin. Samples of the magnetitite flow contain between 12 and 26 wt.% SiO2 and between 45 and 75 wt.% FeO. Rare earth elements (REE) and trace elements from the magnetitite and rhyolite have similar patterns but with lesser abundance in the magnetitite. Both the rhyolite and the magnetitite have light-REE-enriched REE profiles with negative Eu anomalies. Electron microscopic analysis shows that most of the silica and trace element content of the magnetitite flow comes from very finely disseminated silicate minerals and glass in the magnetite. This suggests that the magnetitite was derived from a magma that had undergone unmixing into a silica-rich phase and an iron-rich phase prior to its eruption. Fractures and vesicles within the magnetitite flow contain minor rhyolitic glass and minerals suggesting that the rhyolite magma invaded columnar joints in the solidified magnetitite flow, and is a subvolcanic sill-like body at the studied locality. The magnetitite flow erupted prior to the emplacement of the rhyolite, which may be extrusive on a regional scale. The features of the Nenana magnetitite, and its geological relationships, are consistent with genetic models that invoke unmixing of magma into immiscible Fe-rich and Si-rich liquids during ascent.

SERIES

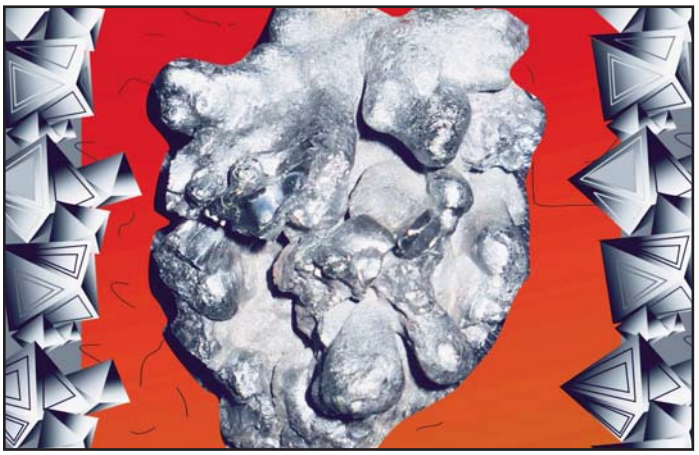

Igneous Rock Associations 29. The Nenana Magnetitite Lava Flow, Alaska Range, Alaska

S.P. Reidel[1], M.E. Ross[2] and J. Kasbohm[3]

[1]Pacific Northwest National Laboratory, Retired,
Present address: 7207 West Old Inland Empire Highway
Benton City, Washington 99320, USA
Email: sreidel105@gmail.com

[2]Professor emeritus, Department of Marine and Environmental Sciences
Northeastern University, Boston, Massachusetts 02115, USA

[3]Department of Earth and Planetary Sciences, Yale University
New Haven, Connecticut 06511, USA

SUMMARY

Magnetitite deposits like El Laco (Chile) are rare and have controversial origins. An unusual magnetitite lava flow overlying a rhyolite unit occurs in the north-central Alaska Range and originally covered ~ 750 km^2 of the Miocene Nenana basin. Dating of the rhyolite and relationships between the magnetitite and sedimentary rocks indicate that both are of Late Miocene age. The magnetitite flow is mainly magnetite with some post-eruptive alteration to hematite. Both the rhyolite flow and the magnetitite flow are vesicular, but the magnetitite flow also has small, millimetre-scale columnar jointing. The vesicular zones in the magnetitite flow grade into massive rock on the scale of a thin section, suggesting a degassing lava origin. Samples of the magnetitite flow contain between 12 and 26 wt.% SiO_2 and between 45 and 75 wt.% FeO. Rare earth elements (REE) and trace elements from the magnetitite and rhyolite have similar patterns but with lesser abundance in the magnetitite. Both the rhyolite and the magnetitite have light-REE-enriched REE profiles with negative Eu anomalies. Electron microscopic analysis shows that most of the silica and trace element content of the magnetitite flow comes from very finely disseminated silicate minerals and glass in the magnetite. This suggests that the magnetitite was derived from a magma that had undergone unmixing into a silica-rich phase and an iron-rich phase prior to its eruption. Fractures and vesicles within the magnetitite flow contain minor rhyolitic glass and minerals suggesting that the rhyolite magma invaded columnar joints in the solidified magnetitite flow, and is a subvolcanic sill-like body at the studied locality. The magnetitite flow erupted prior to the emplacement of the rhyolite, which may be extrusive on a regional scale. The features of the Nenana magnetitite, and its geological relationships, are consistent with genetic models that invoke unmixing of magma into immiscible Fe-rich and Si-rich liquids during ascent.

RÉSUMÉ

Les gisements de magnétitite comme ceux de El Laco (Chili) sont rares et d'origines controversées. Une coulée de lave de magnétitite inhabituelle recouvrant une coulée de rhyolite se trouve dans le centre-nord de la chaîne de l'Alaska et couvrait environ 750 km^2 du bassin miocène de Nénana. La datation de la rhyolite et les relations entre la magnétite et les roches sédimentaires indiquent que les deux sont d'âge Miocène supérieur. La coulée de magnétitite est principalement composée de magnétite avec quelques altérations post-éruptives en hématite. La coulée de rhyolite et la coulée de magnétitite sont toutes les deux vésiculaires, mais la coulée de magnétitite présente également de petits joints colonnaires d'échelle millimétrique. Les zones vésiculaires de la coulée de magnétitite se transforment en roche massive à l'échelle d'une lame mince, suggérant qu'elles proviennent d'une lave en dégazage. Les échantillons de la coulée de magnétitite contiennent entre 12 et 26 % en poids de SiO_2 et entre 45 et 75 % en poids de FeO. Les éléments de terres rares (ETR) et les éléments traces de la magnétitite et de la rhyolite présentent des patrons similaires mais

Geoscience Canada, v. 50, https://doi.org/10.12789/geocanj.2023.50.197 pages 53–71

GC Data Repository: Igneous Rock Associations Series at https://gac.ca/gc-data-repository

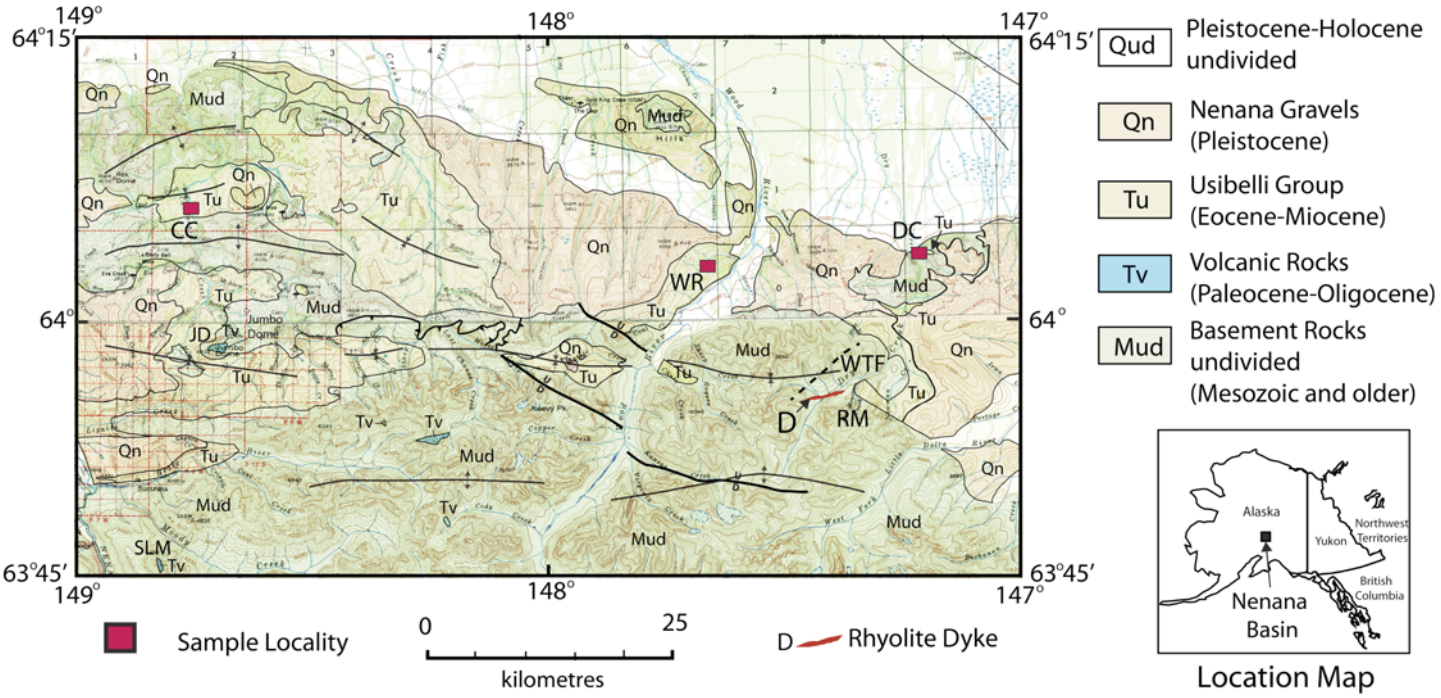

Figure 1. Geologic map of the Nenana Coal Basin, central Alaska Range. Inset map shows the location of the Nenana Coal Basin. Map is based on Wahrhaftig (1970 a,b,c,d,e,f,g,h) and modified from Reidel and Ross (in press). CC, California Creek; DC, Dry Creek; JD, Jumbo Dome; RM, Red Mountain volcanogenic massive sulphide deposit; SLM, Sugar Loaf Mountain; WR, Wood River locality; WTF, volcanogenic massive sulphide prospect. Dyke is that of Freeman et al. 2016.

avec une moindre abondance dans la magnétitite. La rhyolite et de magnétitite présentent toutes deux un patron de terres rares enrichi en éléments de terres rares légers avec une anomalie négative en Eu. L'analyse au microscope électronique montre que la majeure partie de la silice et de la teneur en éléments traces de la coulée de magnétitite provient de minéraux silicatés et de verre finement disséminés dans la magnétite. Ceci suggère que la magnétitite provient d'un magma qui s'était décomposé en une phase riche en silice et une phase riche en fer avant son éruption. Les fractures et les vésicules dans la coulée de magnétitite contiennent du verre et des minéraux rhyolitiques comme constituant mineurs suggérant que le magma de rhyolite a envahi les joints colonnaires dans la coulée de magnétitite solidifiée et est un corps subvolcanique semblable à un filon-couche dans la localité étudiée. La coulée de magnétitite a fait éruption avant la mise en place de la rhyolite, qui peut être extrusive à l'échelle régionale. Les caractéristiques de la magnétitite de Nénana et ses relations géologiques sont cohérentes avec les modèles génétiques qui invoquent la séparation du magma en liquides non miscibles riches en fer et en silicium pendant l'ascension.

Traduit par la Traductrice

INTRODUCTION

Magnetite deposits like El Laco in the Andes Mountains of Chile are rare and have controversial origins. Proposed origins include lava flows (Park 1961; Naslund et al. 2002; Henriquez et al. 2003; Keller et al. 2022; Pietruszka et al. 2023), magmatic assimilation (Bain et al. 2021), replacement (Sillitoe and Burrows 2002, 2003), and as hydrothermal deposits (Dare et al. 2015). Igneous rocks composed of mainly magnetite are called *magnetitite* (Holmes 1928; Johannsen 1938) and can contain apatite as well as a variety of silicate minerals. Similar iron-ore deposits of the Kiruna type occur mainly in Precambrian rocks but also have controversial origins (Frietsch 1978; Parak 1985).

Magnetite deposits are found with a variety of rocks. For example, El Laco typically occurs with andesite; Cerro de Mercado, Mexico, is found with rhyolite (Lyons 1988) and Lakeh Siah in Iran is found in a succession of tuff, rhyolite, limestone and evaporite deposits (Gholipoor et al. 2023).

An unusual magnetitite unit, similar to El Laco, occurs in the glaciated north-central Alaska Range between Healy and Delta Junction and was interpreted as a lava flow (Reidel 1984). The flow occurs in Miocene sedimentary rocks in the Nenana basin. In this paper we describe the occurrence of the lava, here named the Nenana magnetitite flow, present new mineralogical and compositional data, and discuss its possible origin. Numerical geochemical and mineralogical data are not included within this paper but are provided (with other relevant information) as supplementary files in the Geoscience Canada data repository.

Geological Background

The Nenana magnetitite lava flow and an associated rhyolite unit occur within a series of faulted synclines forming the extensional Nenana basin in the north-central Alaska Range (Fig. 1) (e.g. Wahrhaftig 1970a, b, c, d, e, f, g, h). The basin lies north of the Farewell-Denali Fault and within the Tintina Gold Province (not shown in Fig. 1). The north-central Alaska Range consists of an east-west trending eroded complex of Precambrian to Cretaceous greenschist-grade metavolcanic

and metasedimentary rocks that are overlain by Eocene to Holocene sedimentary and volcanic rocks (Wahrhaftig et al. 1969; Kirschner 1994; Dusel-Bacon et al. 2007; Wartes et al. 2013). Associated with the older metavolcanic and metasedimentary rocks are many volcano-plutonic complexes that contain volcanogenic massive sulphide deposits. Two of these deposits occur within the Bonnifield mining district of the Nenana basin (Fig. 1, labels RM and WTF).

Cenozoic sedimentary rocks of the Usibelli Group (Fig. 2) overlie the metavolcanic and metasedimentary rocks and, in turn, are overlain by the Pleistocene Nenana Gravel (Sortor et al. 2021) and glacial deposits. The Usibelli Group ranges in age from Eocene to Miocene and is composed of five formations: Healy Creek, Sanctuary, Suntrana, Lignite Creek and Grubstake (Wahrhaftig 1951, 1987; Wolfe and Tanai 1987; Leopold and Lui 1994; Wilson et al. 1998). Prior to uplift of the Alaska Range in the Miocene, the Usibelli Group was deposited by a southward-flowing drainage that alternated between a coal-forming basin and braided river system. The Usibelli Group sedimentary rocks consist of interbedded poorly consolidated sandstone, conglomerate, claystone and coal.

Two thick ash beds occur in the Grubstake Formation, near the top of the Usibelli Group (Fig. 2). Wahrhaftig et al. (1969) obtained an 8.1 Ma K/Ar radiometric age date on glass in ash from the lower bed. Triplehorn et al. (2000) recalculated the age to be 8.3 Ma using $^{40}Ar/^{39}Ar$ dating of the same glass but considered it to be in error due to excess Ar in the glass. Minerals from the glass were also dated by Triplehorn et al. (2000), who reported a preferred age of 6.7 Ma.

Two volcanic centres are present in the area (Fig. 1): the Jumbo Dome and the Sugar Loaf Mountain rhyolite and andesite. A third, the Buzzard Creek basalt, lies north of the area. Jumbo Dome volcanism is dated at approximately 2.7 ± 0.25 Ma (Wahrhaftig 1970b) but more recently updated to 1.03 ± 0.06 Ma (Athey et al. 2006). Sugar Loaf Mountain is the remnant of a rhyolite flow from which Albanese (1980) obtained a K/Ar age date of 34–32 Ma. The Buzzard Creek basalt is Pleistocene based on it overlying glacial deposits (Péwé et al. 1966). A rhyolite dyke (Fig. 1) of undetermined age lies north of Red Mountain and along Dry Creek (Freeman et al. 2016).

GEOLOGY

The magnetitite flow is exposed as erosional remnants that suggest an original extent estimated at approximately 750 km^2 in the Nenana basin (Fig. 1). The easternmost exposure occurs along a prominent ridge above Dry Creek, and the westernmost locality lies along California Creek in a silty claystone of the Suntrana Formation, as mapped by Wahrhaftig (1970g) but reinterpreted as upper Healy Creek Formation by Wartes et al. (2013). Localities like El Laco and Cerro de Mercado have many separate deposits with associated feeder dykes. In contrast, the Nenana magnetitite flow has no known feeder dyke at any exposure suggesting that the exposures are remnants of a much larger flow.

The magnetitite flow is remarkable in that at every site, the flow has developed small, mm-size columns (Fig. 3) that are typically 4- to 6-sided. The columns can be in contact with other columns or nearly free-standing. Columns are typical in Columbia River Basalt Group (CRBG) basalt flows but not at this small scale. Columns form from slow cooling of the lava (Ross 1989; Reidel et al. 2013) and develop perpendicular and inward from the cooling surfaces. The columns in the Nenana magnetitite flow appear to form inward from its edges.

The Nenana magnetitite lava flow was sampled at three localities (Fig. 1): Dry Creek, California Creek and along the west side of the Wood River opposite Glacier Creek. The Dry Creek locality consists of a 3 m-thick flow along an approximate 100 m east–west exposure. There, the magnetitite overlies a 3 m-thick rhyolite layer that lies upon Mississippian rocks (Beikman 1974) with no exposures of the Usibelli Group nearby. The Dry Creek exposure was mapped as "Pliocene continental deposits" by Beikman (1974) in a compilation map and "Nenana gravels" by Péwé et al. (1966). Due to the remote nature of the outcrops, it is probable that Péwé et al. (1966) never encountered these exposures during their mapping. Any evidence of the Usibelli Group coal-bearing rocks has been removed by erosion, but this exposure has a significant aeromagnetic anomaly (Fig. 4).

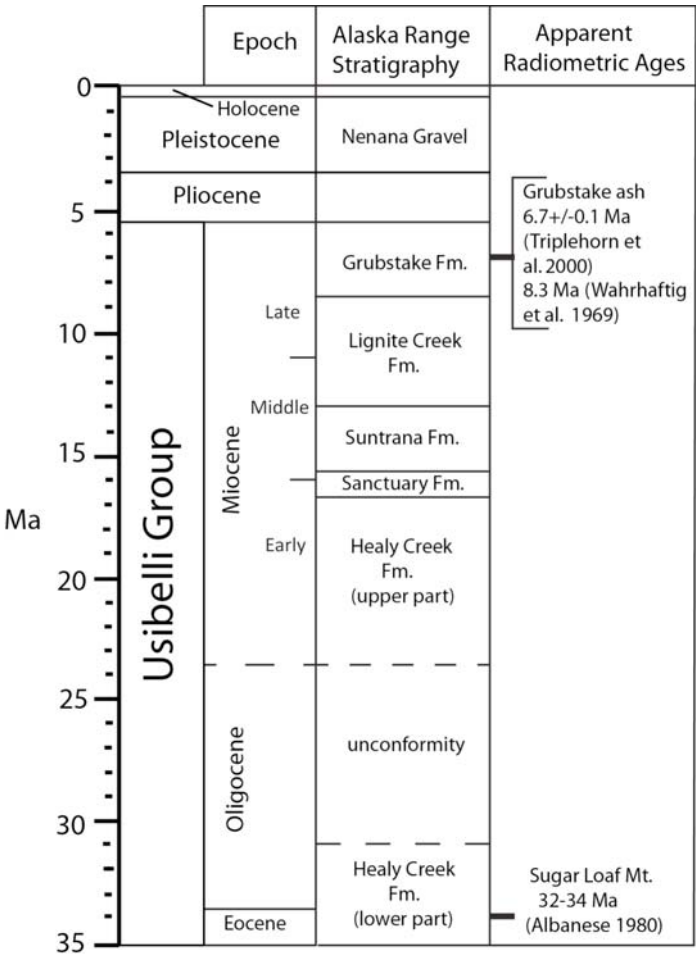

Figure 2. Stratigraphy of the Nenana basin, central Alaska Range. Modified from figure 3 of Triplehorn et al. (2000).

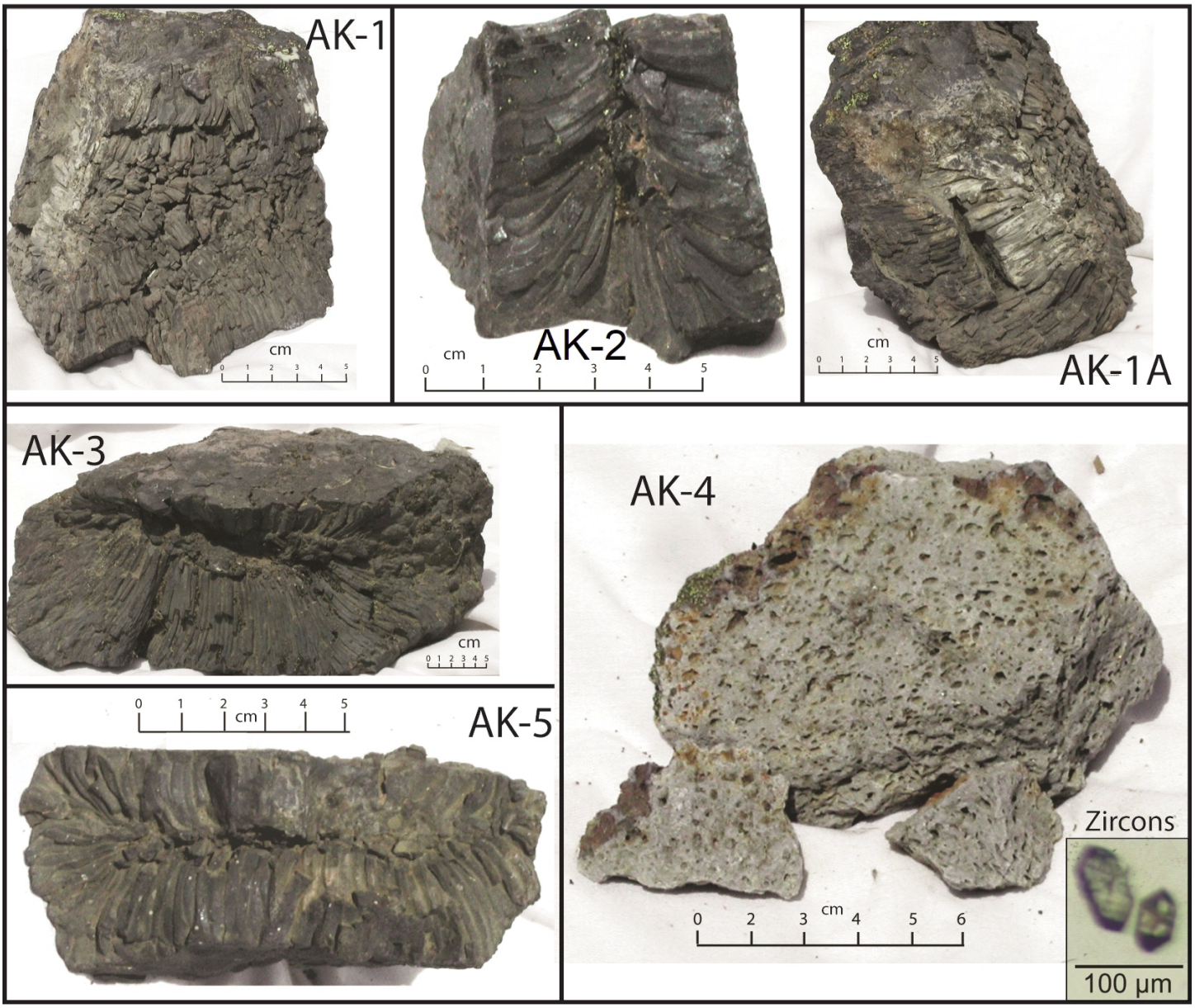

Figure 3. Samples of the magnetitite flow and rhyolite from the Nenana basin, north central Alaska Range. Sample numbers designate analyses and descriptions throughout the paper. Samples AK-3, AK-4, and AK-5 are from the Dry Creek locality (DC, Fig. 1) and samples AK-1 and AK-2 are from the California Creek locality (CC, Fig. 1). Dated zircon grains from the rhyolite are shown in lower right corner of sample AK-4.

The other two magnetitite localities are within the Usibelli Group; however, neither is associated with an underlying rhyolite unit like that seen at the Dry Creek site. At the westernmost locality in California Creek the magnetitite flow appears to have invaded the Miocene sediments, displacing and incorporating them while forming a sill-like layer several centimetres thick. This exposure is like localities in the CRBG where lava flows burrowed into wet sediment producing an 'invasive basalt flow' like that described by Ross (1989) and Reidel et al. (2013). Invasive CRBG flows are common where the basalt erupted onto thick, unconsolidated sediment and are interpreted to represent an extrusive setting. The lava flows burrowed into the sediment and baked the sediment at their mutual contacts. The California Creek site reveals closely similar relationships to these invasive basalt flows, and has a significant aeromagnetic anomaly (Fig. 4) implying that magnetitite is locally extensive.

The third locality is on the west side of Wood River opposite Glacier Creek in either the Suntrana or Lignite Creek Formation as mapped by Wahrhaftig (1970e). This site is poorly exposed and is not marked by an aeromagnetic anomaly.

The rhyolite at the Dry Creek site is primarily a white, massive rock with vesicles throughout (Fig. 3). There are no columnar structures or evidence of obvious flow banding, but it resembles rhyolite flows seen elsewhere in the area. It appears to be an isolated outcrop but mapping by Freeman et al. (2016) identified a rhyolite dyke in Dry Creek about 10 km to the south (Fig. 4). They described the exposure as a "rhyo-

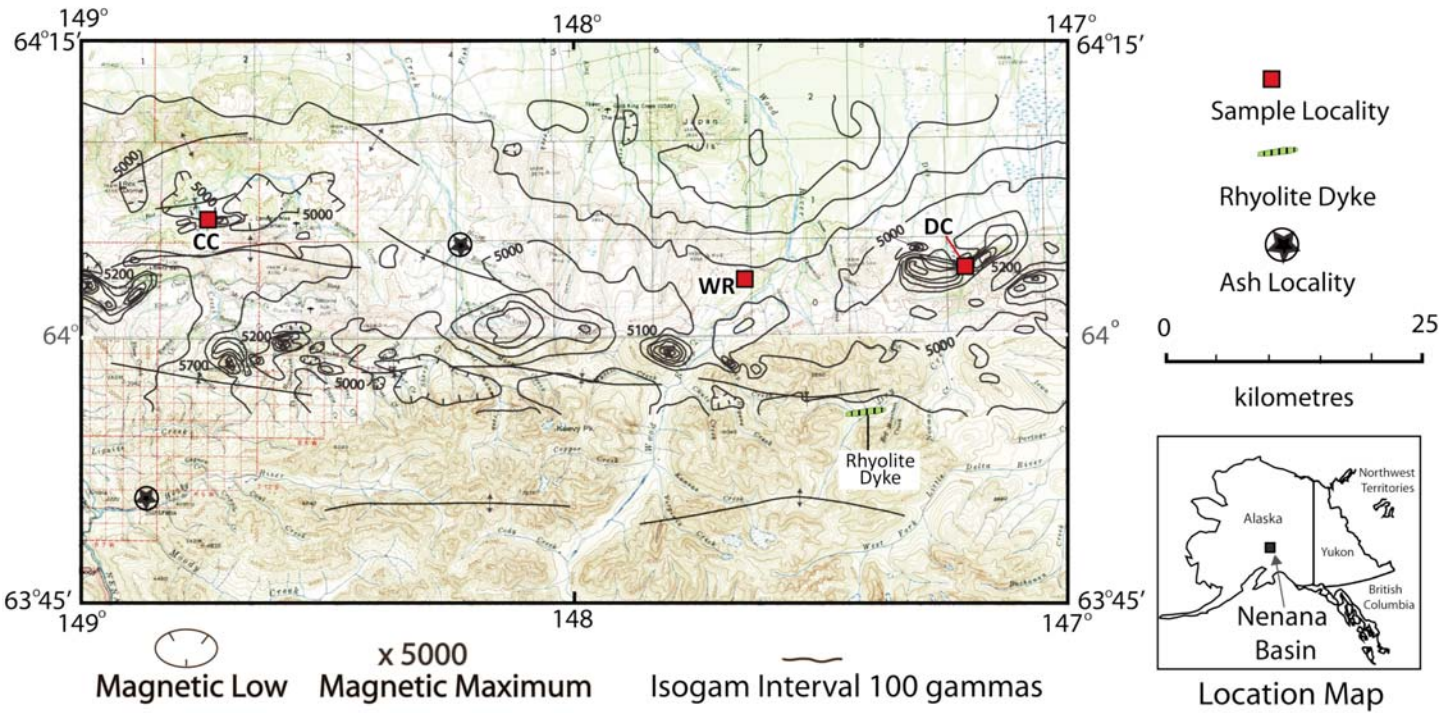

Figure 4. Aeromagnetic map of the Nenana Basin, northern Alaska Range. From Alaska Division of Geology and Geophysical Surveys 1973a, b.

lite breccia dyke". It is white to tan and aphanitic with clasts of schist and pumice; local banding is present along the margins. It forms exposures that cross Dry Creek west of Red Mountain Creek (RM, Fig. 1). No radiometric age was available, but they suggested that it may be equivalent to the Oligocene rhyolite of Sugar Loaf Mountain 48 km to the west (Fig. 1). Its physical similarity and close proximity to the rhyolite underlying the magnetitite flow at Dry Creek indicate that it may be its feeder dyke.

ANALYTICAL METHODS

Mineralogical and Geochemical Analyses

Optical microscopic properties of most minerals identified are listed in the supplementary data for the paper. Percentages of minerals and glass were determined by standard modal analysis. Very few grains were both large enough and oriented correctly for flat-stage measurements.

Microprobe analyses for samples AK-2, AK-3, AK-4, and AK-5 are listed in supplementary data. These were performed by Dr. James Eckart at Earth Materials Characterization Lab, Yale University. Operating conditions: JEOL JXA-8530F; SDD (silicon drift detector) EDS detector: Silicon Drift X-ray detector with 10 mm active area; 133 eV resolution. Analysis beam voltage 15 kV, beam current 10 mA. Microprobe analyses and scanning electron microscopy (SEM) images of sample AK-1 were performed by B. Strope at the Rockwell International Electron Microprobe Laboratory, Richland, Washington on a JEOL electron microprobe. Operating condition: 15 kV. Beam current 10 mA, EDS analysis.

Whole-rock XRF analyses are listed in supplementary data. These were performed by Dr. Rick Conrey at the WSU Peter Hooper GeoAnalytical lab. The methods and procedures are described in Johnson et al. (1999). Inductively coupled plasma–mass spectrometry (ICP–MS) trace-element analyses were performed by Charles Knaack at the WSU Peter Hooper GeoAnalytical lab. Procedures are described on their website.

Geochronology

An attempt was made to determine an age using U–Pb zircon geochronology through chemical abrasion–isotope dilution–thermal ionization mass spectrometry at Princeton University, following methods described in Kasbohm and Schoene (2018).

Zircon grains were separated from their host rock through standard methods of crushing, gravimetric, and magnetic separation techniques using a Bico Braun "Chipmunk" Jawcrusher, disc mill, hand pan, hand magnet, Frantz isodynamic separator, and methylene iodide. Zircon grains from the least magnetic and most dense mineral separate were transferred in bulk to quartz crucibles and annealed in a muffle furnace at 900°C for 48 hours after Mattinson (2005). After annealing, grains were photographed (Fig. 3) and picked in reagent-grade ethanol for analysis. Given the low radiogenic Pb content of the samples, cathodoluminescence images were not obtained. Individual grains were transferred using stainless steel picking tools to separate 3 mL Savillex Hex beakers containing distilled acetone and taken to the clean lab for analysis.

Single zircon grains were loaded into 200 μL Savillex "micro"-capsules with 100 μL 29 M HF + 15 μL 3N HNO_3 for a single leaching step in high-pressure Parr bombs at 185°C for 12 h to remove crystal domains affected by Pb loss (Mattinson 2005). Grains were rinsed post-leaching in 6 N HCl, MQ H_2O, 3N HNO_3, and 29 M HF prior to spiking with EARTHTIME ^{205}Pb–^{233}U–^{235}U tracer and addition of 100 μL

29 M HF + 15 μL 3N HNO_3 (Condon et al. 2015; McLean et al. 2015). Zircon grains were then dissolved to completion in Parr bombs at 210°C for 48 h. Dissolved zircon solutions were subsequently dried down, dissolved in 100 μL 6N HCl, and converted to chlorides in Parr bombs at 185°C for 12 h, after which solutions were dried again and brought up in 50 μL 3N HCl. The U–Pb and trace element aliquots were then separated by anion exchange chromatography using 50 μL columns and AG-1 X8 resin (200–400 mesh, chloride from Eichrom) (Krogh 1973), and dried down with a microdrop of 0.015 M H_3PO_4. The dried U and Pb aliquot was loaded in a silica gel emitter (Gerstenberger and Haase 1997) to an outgassed zone-refined Re filament.

Isotopic determinations were performed using an IsotopX PhoeniX-62 thermal ionization mass spectrometer (TIMS) at Princeton University, with Pb analysis performed in peak-hopping mode on a Daly-photomultiplier ion-counting detector. Analyses are listed in supplementary data. A correction for mass-dependent Pb fractionation was applied using a Pb fractionation of 0.182 ± 0.041%/amu, as determined by repeat measurements of NBS982 at Princeton. A Daly-photomultiplier deadtime of 28.8 ns was used, as determined by repeat measurements of NBS standards. Corrections for interfering isotopes under masses 204 and 205 were made cycle-by-cycle by measuring masses 201 and 203 and assuming they represent $^{201}BaPO_2$ and ^{203}Tl and using natural isotopic abundances to correct for $^{204}BaPO_2$, $^{205}BaPO_2$, and ^{205}Tl.

UO_2 measurements were performed in static mode on Faraday cups with a bulk U fractionation correction calculated from the deviation of measured $^{233}U/^{235}U$ from the known tracer $^{233}U/^{235}U$ (0.995062 ± 0.000054 (1σ)), and an oxide composition of $^{18}O/^{16}O$ of 0.00205 was used (Nier 1950). Data reduction was performed using the programs Tripoli and U–Pb Redux (Bowring et al. 2011; McLean et al. 2011) and the decay constants of Jaffey et al. (1971). All common Pb was attributed to laboratory blank with a mean isotopic composition determined by total procedural blank measurements. Uncertainties in reported U–Pb zircon dates are at the 95% confidence level and exclude tracer calibration and decay constant uncertainties.

RESULTS

Age of Formation

Although we have no means of dating the magnetitite flow, we attempted to obtain a U–Pb zircon age for the associated rhyolite (sample AK-4; Fig. 3). From a small hand sample, six zircon grains smaller than 100 μm were separated through standard methods, and of these, two were dated (the rest were lost at some stage of zircon chemistry prior to dating). Both grains were low in uranium and yielded very imprecise Th-corrected $^{206}Pb/^{238}U$ ages of 15.31 ± 0.52 Ma and 11.12 ± 0.65 Ma, with low ratios of radiogenic to common Pb (0.331 pg Pb*/1.08 pg Pbc = 0.31, and 0.0637 pg Pb* / 0.36 pg Pbc = 0.17, respectively). Because of the imprecision of these dates, their dispersion, and the protracted crystallization of zircon in a magma chamber prior to eruption (Miller et al. 2007; Simon et al. 2008) we do not consider either of these dates to be the actual age of the rhyolite. Nonetheless, the data do suggest a maximum Tortonian (Late Miocene) age for the rhyolite at Dry Creek. It is possible that processing a larger volume of this sample for zircon geochronology would yield a greater number of larger zircon grains from which more precise U–Pb dates could be obtained, which we would suggest for future work.

Empirical field evidence suggests that both the magnetitite flow and associated rhyolite are of Miocene age, consistent with our rhyolite zircon dates. The magnetitite flow is invasive into the Miocene Usibelli Group at California Creek. In addition, we suggest that the rhyolite may also be the source for the two ash beds (Figs. 1, 2) that occur in the Usibelli Group, as indicated in Fig. 4. The age of 6.7 Ma for glass minerals from the lower ash obtained by Triplehorn et al. (2000) may thus be consistent with our imprecise upper age boundary suggested by zircon geochronology. Thus, we conclude that the rhyolite and the closely associated magnetitite flows are of Late Miocene age.

Mineralogy and Petrology

Selected minerals and/or glasses were identified optically in the magnetitite samples (AK-1, AK-2, AK-3 and AK-5) and the rhyolite sample (AK-4) and were analyzed by electron microprobe to determine their compositions. Minerals identified in the magnetitite and rhyolite samples are shown in figures 5 through 13.

Magnetitite Petrography

The minerals identified in the magnetitite flow include magnetite, augite, chlorite, olivine, biotite, quartz, apatite, rutile, sanidine, and muscovite. The magnetitite consists predominately of magnetite (Figs. 5a, 6b, 7, and 8a) with minor silicate minerals occurring as tiny (< 0.1 mm) anhedral to subhedral grains confined to vein-like ragged vesicles, cooling joints (Figs. 5b and 6b), and a few, irregular, partly rounded, more open vesicles (Figs. 5c and 7b). Most of the vesicles and joints are barren, containing small amounts of silicate minerals and magnetite (Fig. 6b) in clusters or as discrete grains scattered along their lengths. These minerals most often line the walls of the vesicles and joints. Highly vesicular zones (Fig. 5d) in the magnetitite consist of small, equant to irregular, barren vesicles locally, suggesting vesiculation in an extrusive environment.

Estimating the 2V or sign of a mineral was only possible on a few small grains of quartz, plagioclase, hornblende, and sanidine. Sanidine grains were verified in magnetitite samples AK-2 and AK-5 by microprobe analyses (Figs. 8c and 9a). A few tiny, moderately birefringent grains are probably augite with one grain in sample AK-1 (Fig. 9c) providing a biaxial, optically positive interference figure. Brown, weakly pleochroic anhedral grains were identified as chlorite by microprobe analyses. Colourless rhyolite glass was observed only in a small lens-shaped vesicle and along cleavage partings in a sanidine grain in sample AK-5 (Figs. 8a, 8c and 9a). Microprobe analysis identified olivine and augite in sample AK-1. Acicular, dark red needles of rutile occur in a tiny, lens-shaped vesicle in sample

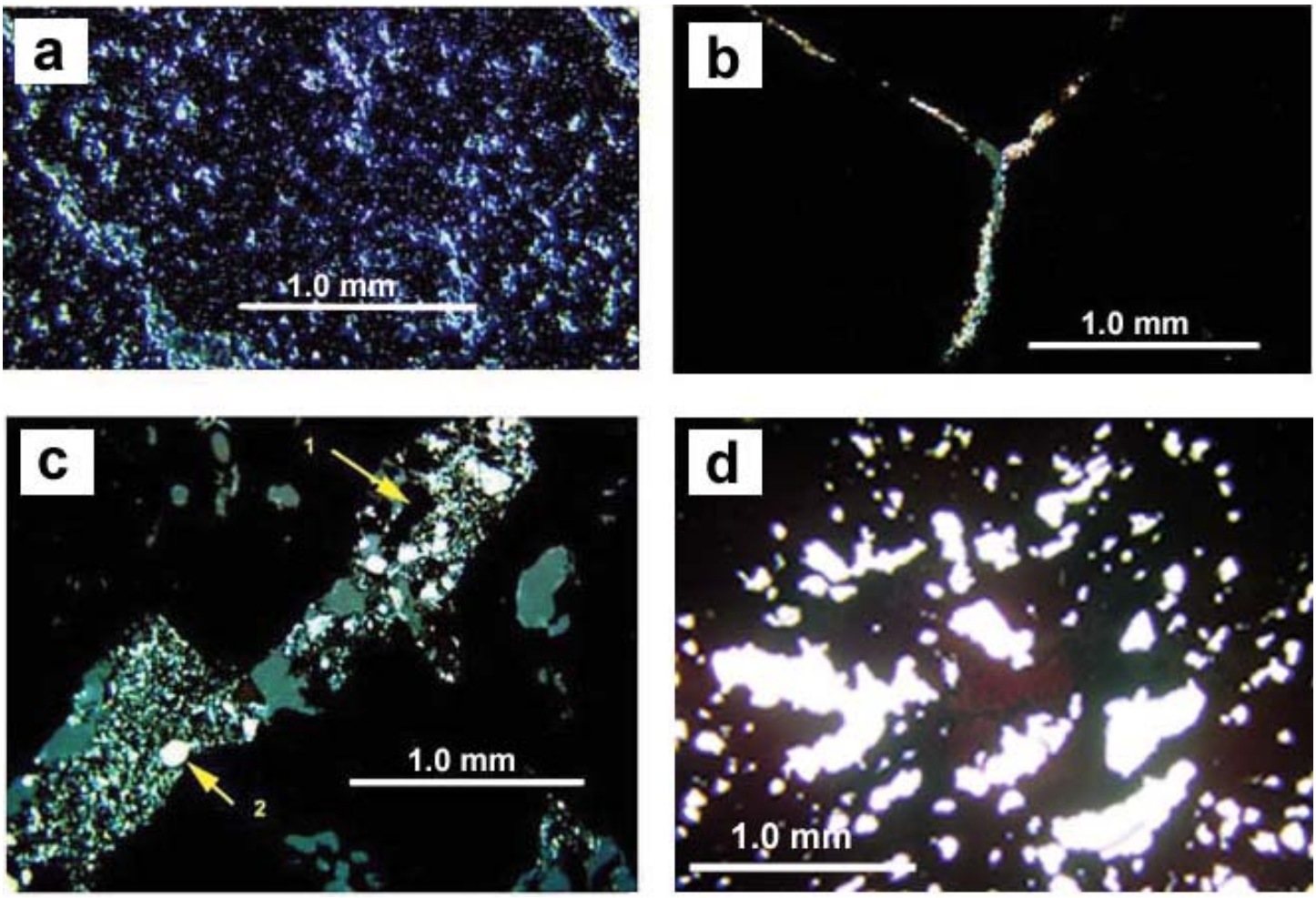

Figure 5. Photomicrographs of the magnetitite flow. (a) Magnetite in sample AK-1 in reflected light. Non-reflective areas are hematite alteration. (b) Cooling joints in AK-2 are partially filled with silicate phases. The brownish grains are chlorite. The angles of intersection of the joints are produced by small-scale columnar jointing (see Figure 3). (c) An elongate, partially rounded vesicle in AK-3 filled with quartz, magnetite (1), and alkali feldspar (2) viewed under crossed polars. (d) A highly vesicular zone in AK-2 resulting from degassing of the magnetitite flow.

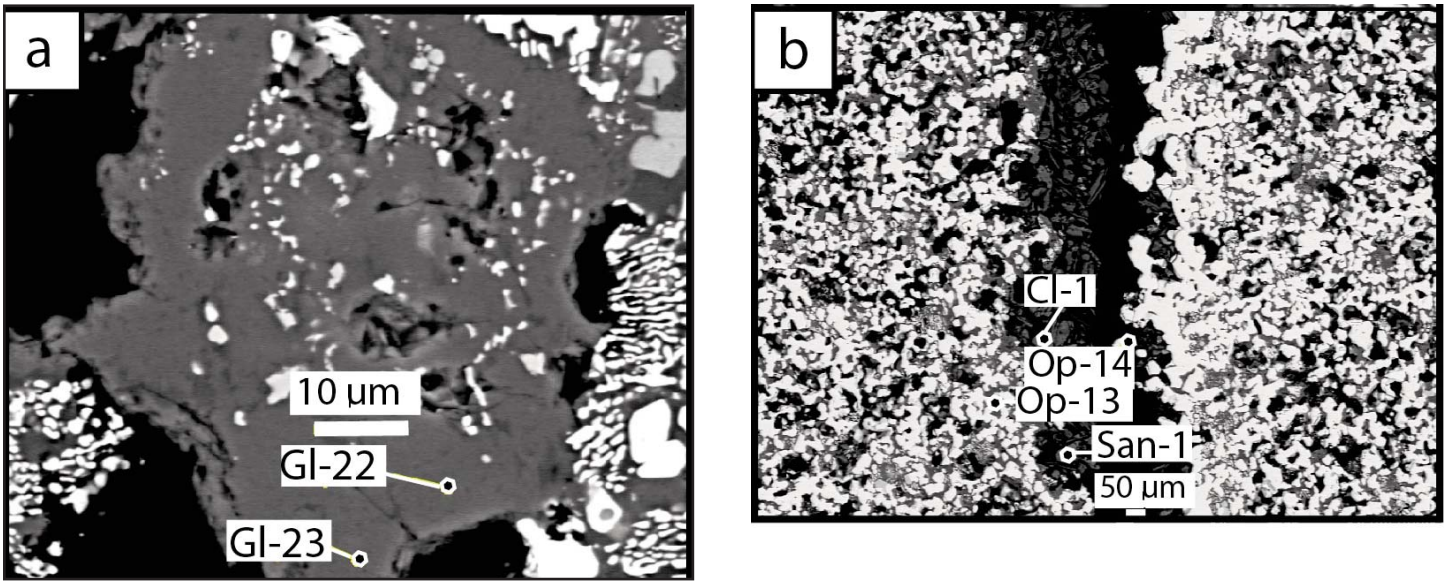

Figure 6. Scanning electron microscope photomicrographs showing sites analyzed in AK-2. (a) Gl-22 and Gl-23 are rhyolite glass adjacent to a sanidine grain. Myrmekite is visible along the right and left margins of the image. (b) Cl-1 is chlorite, Op-13 and Op-14 are magnetite, and San-1 is sanidine.

https://doi.org/10.12789/geocanj.2023.50.197

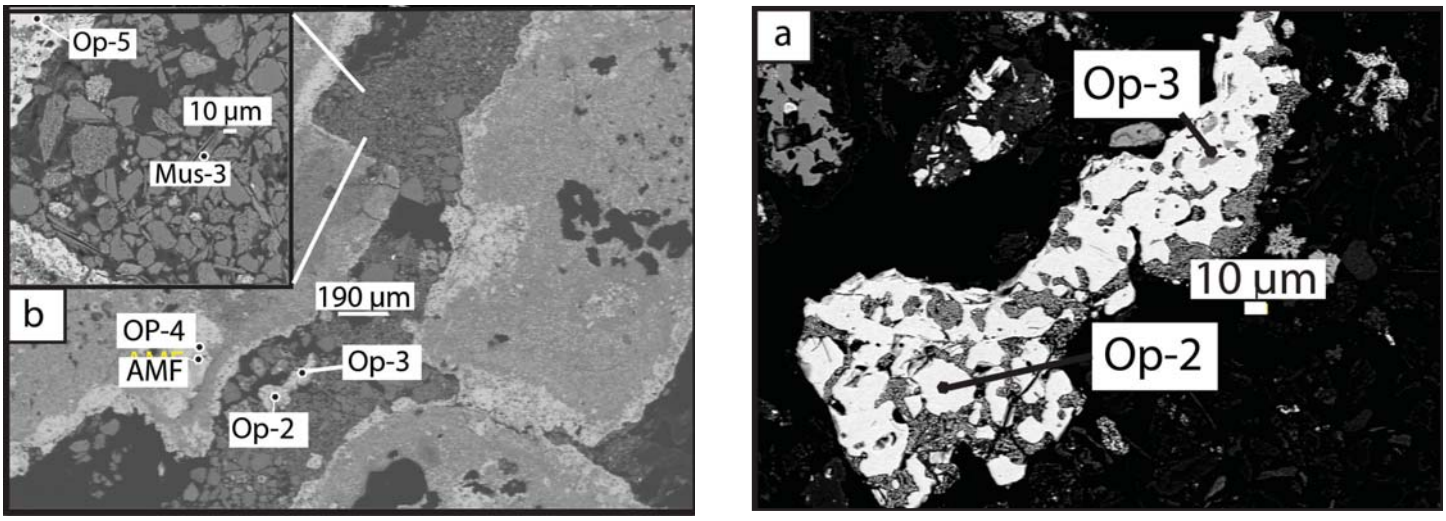

Figure 7. Scanning electron microscope photomicrograph showing sites analyzed in AK-3. (a) Op-2 and Op-3 are magnetite grains within glass with tiny inclusions. (b) Analyzed site in AK-3 in same vesicle shown in Figure 5c. Op-4 and Op-5 are magnetite, Mus-3 is muscovite, and AMF is unknown opaque mineral.

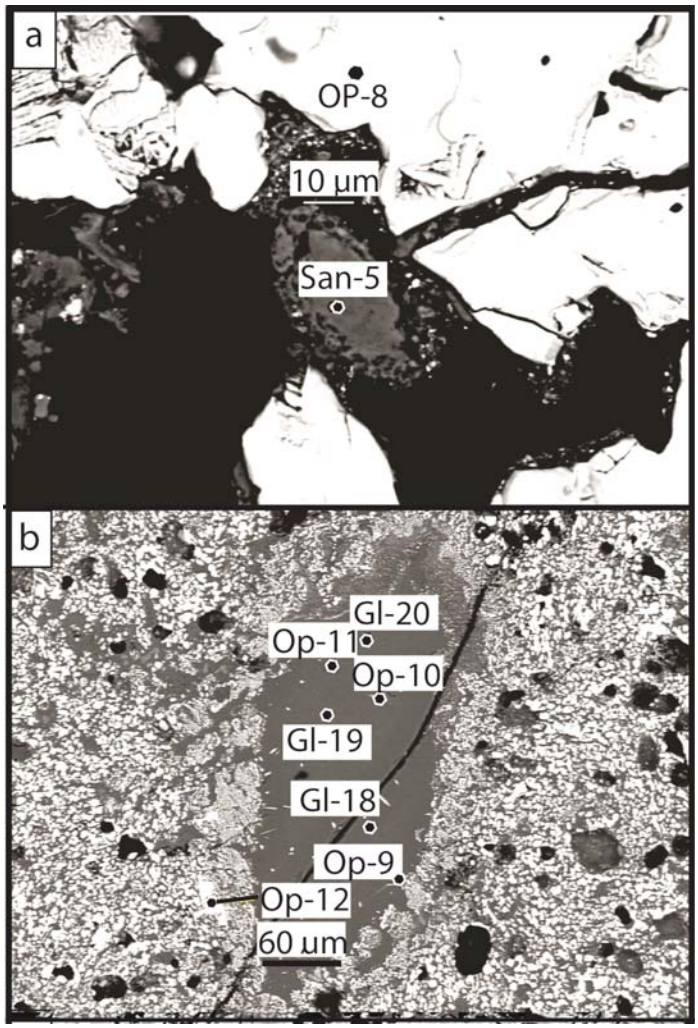

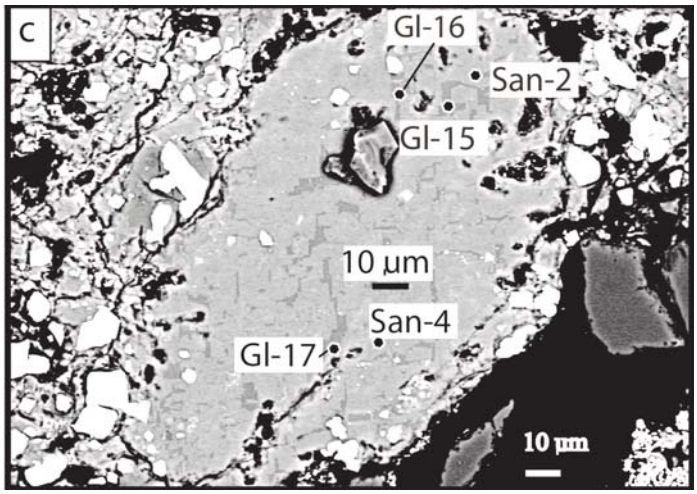

Figure 8. Scanning electron microscope photomicrograph showing sites microprobed in the magnetitite flow (AK-5). San = sanidine; other symbols as in Figure 7. Darker, thin, linear areas in the sanidine in 8c are glass-filled cleavage fractures.

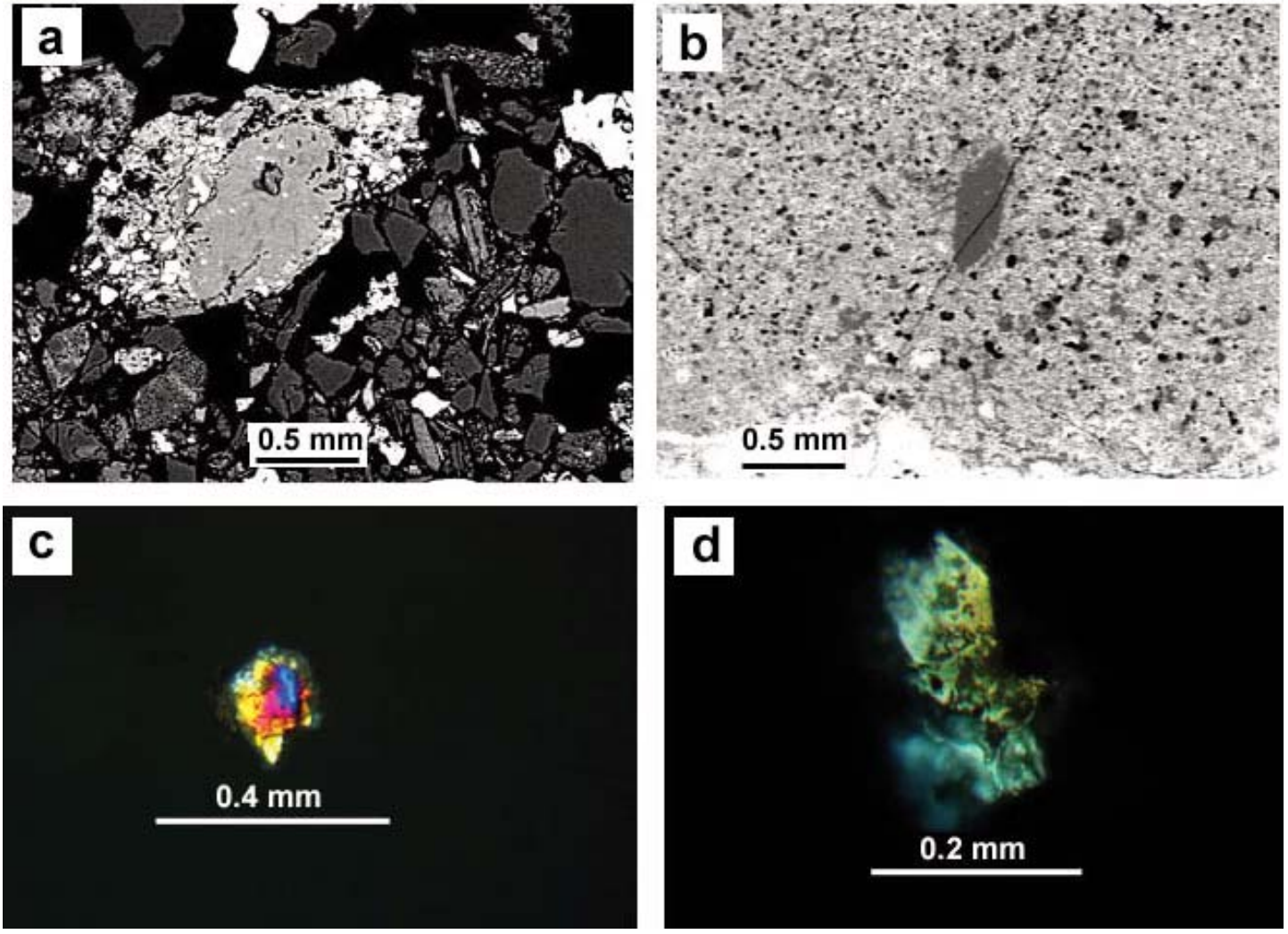

Figure 9. Photomicrographs. (a). Sanidine shown in Figure 8c in reflected light. (b). Rhyolite glass in lens-shaped vesicle in AK-5 (plane-polarized light). See Figure 8c for sites analyzed. An augite grain (c) and quartz grain (d) sampled by scraping from a joint surface in hand specimen AK-1 (Figure 3). Crossed polars.

AK-5 (Fig. 10a). A uniaxial negative, low birefringent, anhedral grain in a vesicle in AK-5 may be apatite (Fig. 10b).

Rhyolite Petrography

The minerals identified in the rhyolite include magnetite, ilmenite, augite, chlorite, hornblende, plagioclase, alkali feldspar/sanidine, muscovite, quartz, and apatite (Fig. 11). Overall, the silicate minerals in the rhyolite resemble those observed in the magnetitite flow.

The rhyolite is vesicular, but vesicles are rounded and smooth-walled in contrast to those in the magnetitite flow (Fig. 12). Colourless rhyolite glass makes up over 92 vol.% of the rock (Fig. 12). Silicate phases identified in the rhyolite glass itself are plagioclase, augite, alkali feldspar/sanidine, and quartz (Fig. 13). Only a trace of augite and 1.6 vol.% feldspar were recognized in the rhyolite whereas magnetite and ilmenite make up a combined 2.5 vol.%. Magnetite in the rhyolite is generally equant but locally is dendritic adjacent to vesicles (Fig. 12c). Ilmenite forms as more elongate grains in the glass (Fig. 12d). Only one tiny plagioclase grain was identifiable in the glass itself and exhibited albite twinning providing an estimated (Michel-Levy method) anorthite content of 36% (andesine). Microprobe data indicate that the plagioclase ranges from andesine to labradorite. Abundant, small, irregular fragments of pumice are present in the rhyolite glass. Small, dark, irregular to tabular bodies are also present in the glass and are interpreted to be metasedimentary and/or sedimentary fragments that were derived from the basement rock. Minerals are present within a few vesicles as scattered clusters or discrete grains of sufficient size for tentative identification optically. They include quartz, feldspar, magnetite, ilmenite, biotite, muscovite, augite, chlorite, and hornblende (Figs. 12 and 13). The presence of muscovite, augite, hornblende, and chlorite was also verified by microprobe analyses. A single, uniaxial (sign indeterminate), anhedral, tiny grain with extreme birefringence is present in a vesicle and may be calcite or zircon. Trace amounts of an unidentified, deep blue mineral of unknown composition occurs in vesicles in AK-4 (Fig. 10 c and d). It is tabular, nonpleochroic, and has parallel extinction.

https://doi.org/10.12789/geocanj.2023.50.197

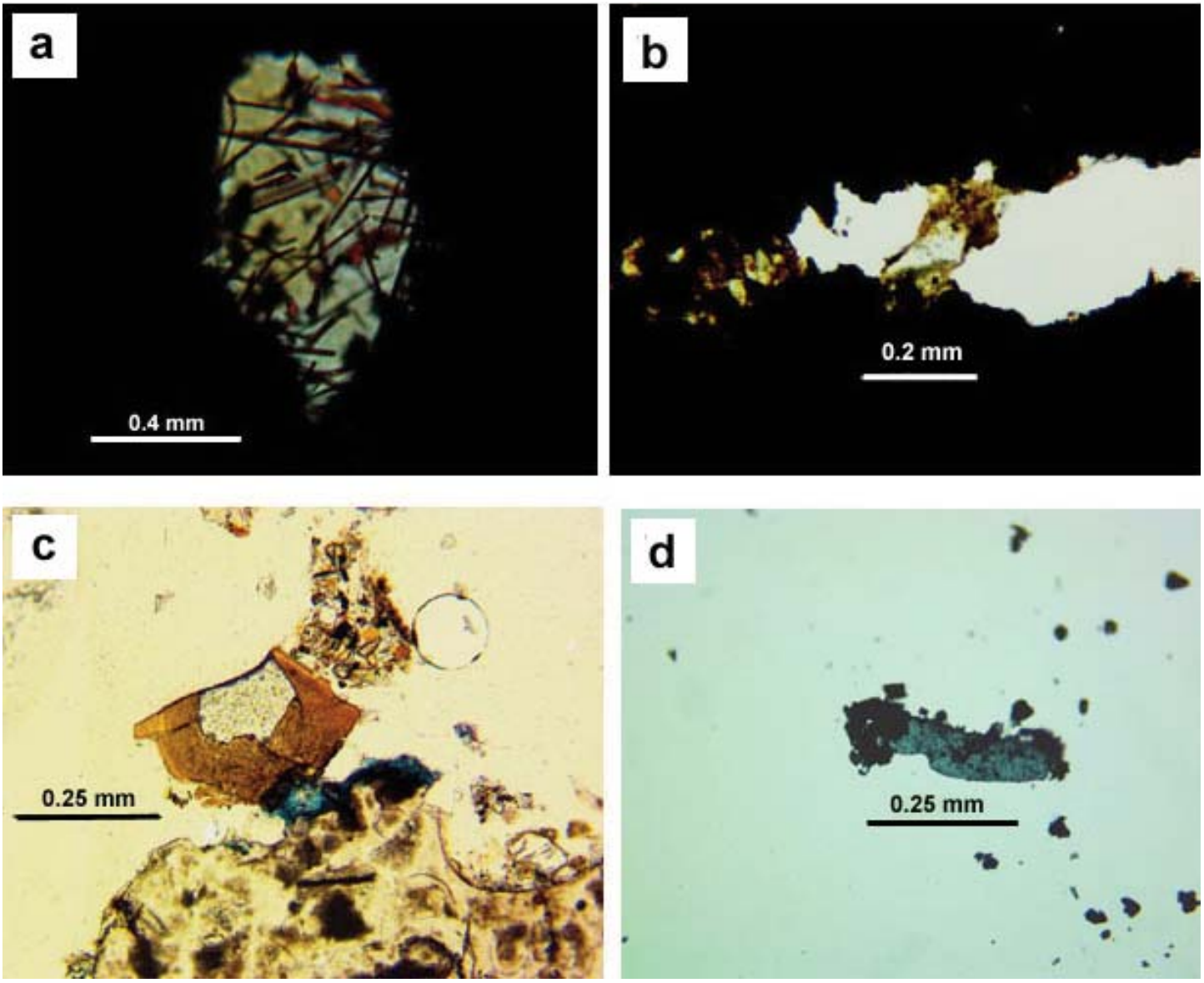

Figure 10. Photomicrographs of unusual grains in AK-5 and AK-4 (all in plane-polarized light). (a) Needles of rutile in a vesicle in AK-5. (b) Probable apatite (uniaxial negative, low birefringence) grain in fracture in AK-5. (c) Unidentified blue mineral in a vesicle with a brown glass fragment in the rhyolite (AK-4). (d) Unidentified blue mineral sampled by scraping from a vesicle in hand specimen AK-4 (Figure 3).

Opaque Mineral Compositions

Three opaque minerals were identified in magnetitite and rhyolite: magnetite, ilmenite and an unknown iron–magnesium–aluminum opaque mineral. The latter was found only in the magnetitite flow. The magnetite compositions in magnetitite and rhyolite are similar. They have 95–99 wt.% FeO with typically < 1 wt.% SiO_2, MnO, MgO and V_2O_5. Al_2O_3 ranges from detection limits to 3.2 wt.%. Ilmenite was identified only in the rhyolite (Figs. 11c, 12d); it has ~ 50 wt.% FeO and TiO_2 and detectable CaO, MgO and SiO_2. The third opaque mineral, termed AMF, occurs in magnetitite flow samples AK-1 and AK-3 (AMF, Fig. 7b). It has 50–70 wt.% FeO, 20 wt.% MgO and ~17 wt.% Al_2O_3. SiO_2 is typically < 1 wt.%. We have been unable to make a positive identification of this mineral, although it may be some type of spinel.

Glass Compositions

Glass occurs in all samples of the magnetitite flow (AK-1, AK-2, AK-3 and AK-5) and in the rhyolite (AK-4). Five glass analyses were obtained from magnetitite sample AK-1; three lie within the dacite field and have high iron contents (~ 9–9.7 wt.%), whereas two lie within the rhyolite field (Fig. 14). One of these latter analyses was obtained from a glass inclusion in a plagioclase grain, and one is groundmass material. The three analyses that plot in the dacite field have lower Na_2O, and K_2O but higher FeO contents (9.0–9.7 wt.%) compared to those plotting in the rhyolite field. Three andesite analyses from AK-4 are from a single glass clast in a vesicle (Fig. 12b, grain 1) that was distinguished optically from other glass analyzed by its occurrence and brown colour. Two other analyses from AK-4 lie in the rhyolite field.

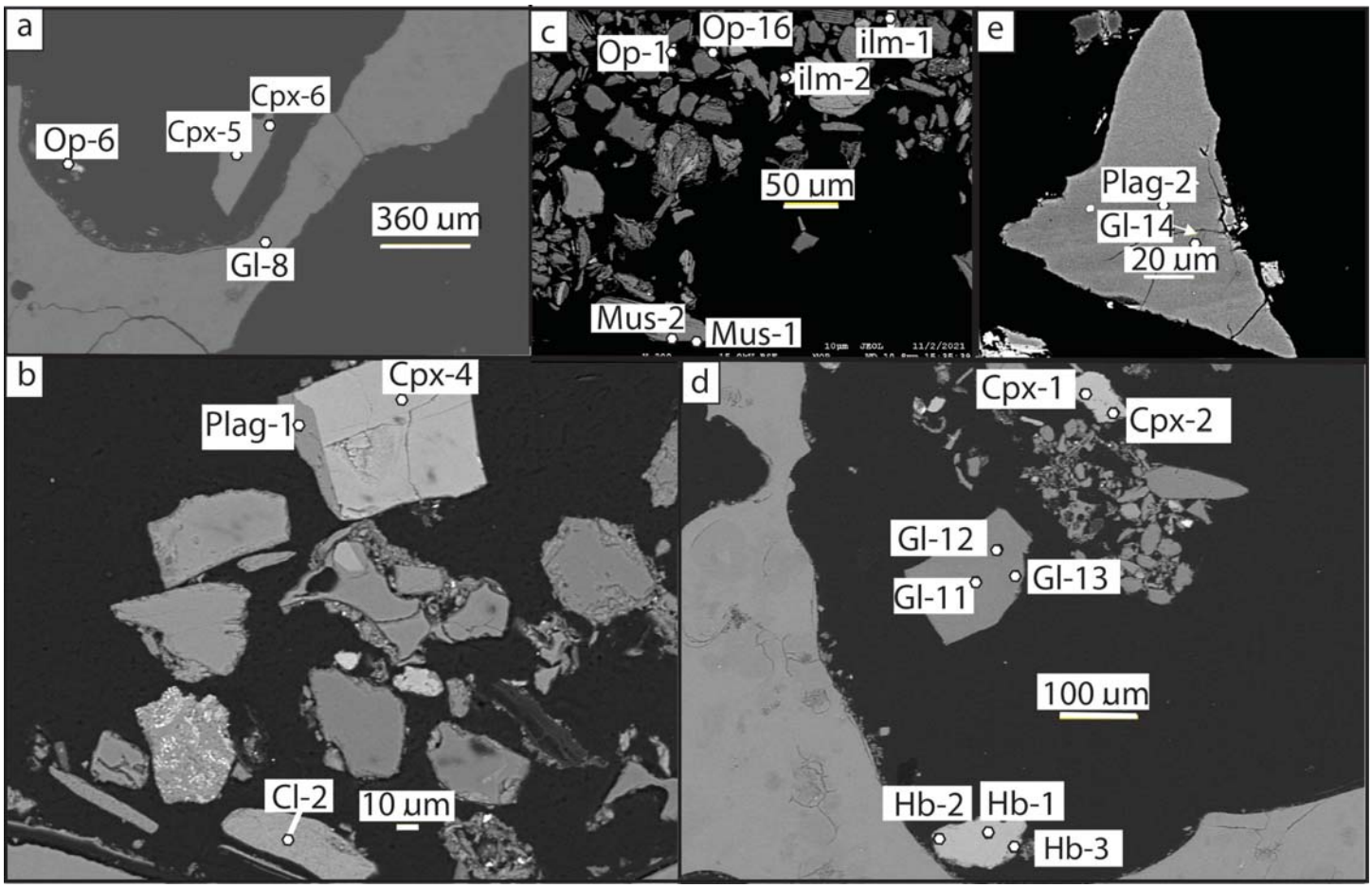

Figure 11. Scanning electron microscope photomicrographs of grains in vesicles microprobed in the rhyolite (AK-4). Symbols as follows: Cl = chlorite, Cpx = clinopyroxene, Gl = glass, Hb = hornblende, ilm = ilmenite, Mus = muscovite, Op = magnetite, Plag = plagioclase.

Four glass occurrences were analyzed by electron microprobe in magnetitite sample AK-2. Two lie within the rhyolite field and two lie within the trachyte–andesite field (Fig. 14). However, the latter two analyses were at the edge of a feldspar grain and may not be pure glass as they have higher Al_2O_3 and K_2O suggesting the analysis may have included feldspar. Six glasses were analyzed in a vesicle in magnetitite sample AK-5 and all lie within the rhyolite field (Fig. 14).

Rock Compositions

The magnetitite and rhyolite compositions are listed in supplementary data and illustrated in Figure 15. The SiO_2 and Al_2O_3 contents of the rhyolite are typical of most such rocks and it contains only minor Na_2O and K_2O. All other oxides are less than 1% by weight.

The four magnetitite samples have varying amounts of FeO (as total Fe) and SiO_2 with FeO ranging between 79.1 and 56.9 wt.% and SiO_2 ranging between 28.1 and 12.3 wt.%. Al_2O_3 is typically between 8.3 and 4.7 wt.% whereas all other oxides are less than 1 wt.% except for MgO which is between 1.5 and 3.5 wt.%. On Figure 15, there is a strong correlation between FeO and SiO_2, Al_2O_3, CaO, Th and Zr in both rhyolite and magnetitite whereas a correlation is present only in magnetitite for MgO, TiO_2 and P_2O_5.

Rare earth elements (REE) are plotted in Figure 16a following Sun and McDonough (1989). The REE patterns for the magnetitite samples and the rhyolite are similar with magnetitite generally showing lower REE contents than rhyolite. All analyses show enrichment in light REE and a depletion of Eu, especially for the rhyolite. The magnetitite and rhyolite samples are also plotted with respect to Bulk Earth abundance (Fig. 16b) following Hickey et al. (1986). Patterns for both are similar with significant depletions in Nb, Sr and TiO_2 suggesting that the magnetitite flow and the rhyolite may come from the same source. However, the relatively high SiO_2 content of the magnetitite flow is problematic as silica and other major, minor and trace elements do not enter magnetite and the Nenana magnetitite flow contains only minor amounts of optically visible silicate minerals. Figure 17 shows a 2000x magnification of a scanning electron microscope image and 'backscatter X-ray' images for a magnetite grain in sample AK-1. These show that silica glass and silicate minerals are finely disseminated throughout the magnetite but would not be visible under an optical microscope even at the highest magnification (400x). Silica and other major and trace elements revealed by the whole rock analyses of the magnetitite appear to have been incorporated into magnetite as it formed from the magma.

https://doi.org/10.12789/geocanj.2023.50.197

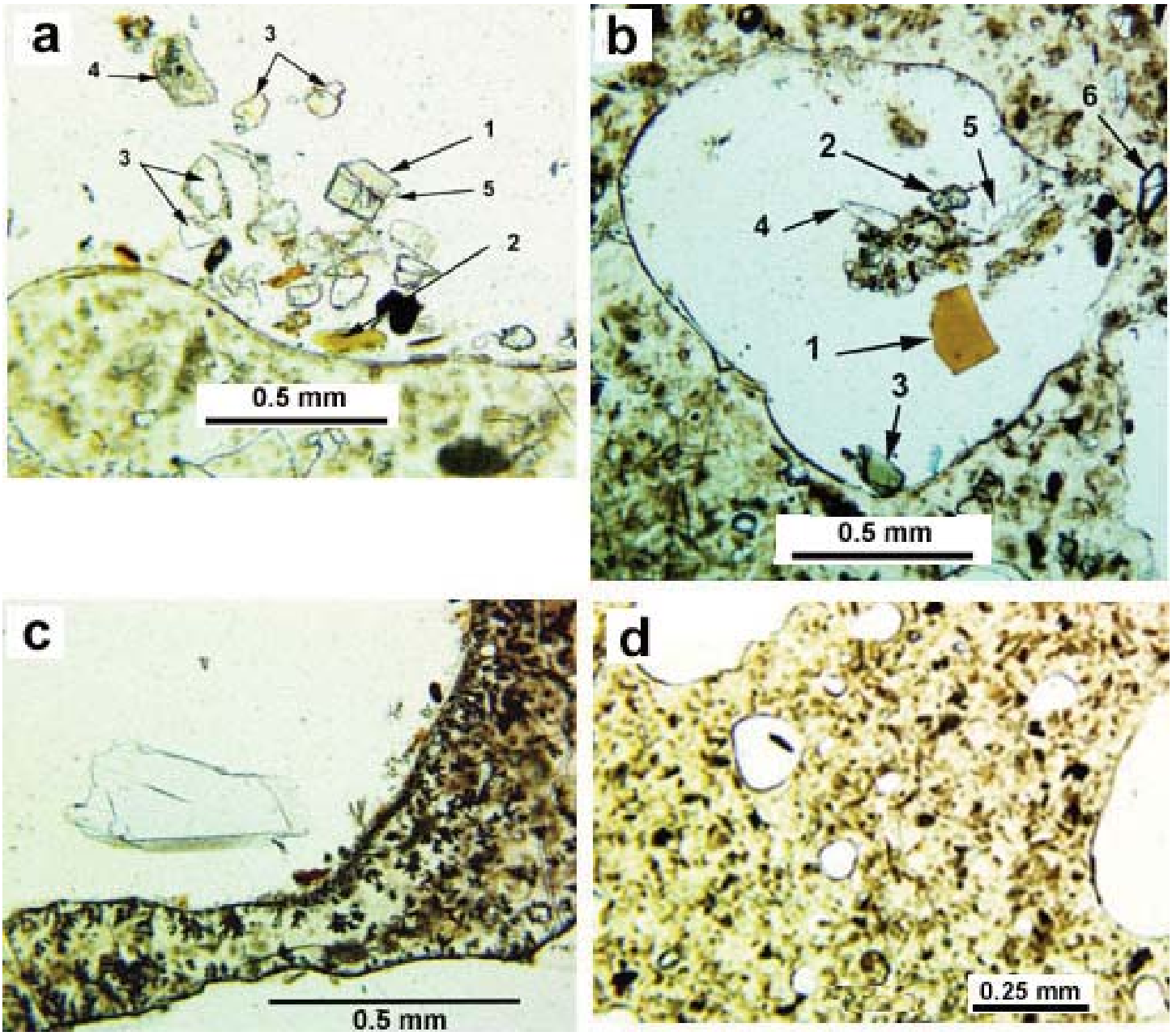

Figure 12. Photomicrographs of the rhyolite (AK-4), all in plane-polarized light. (a) A vesicle containing augite (1), chlorite (2), quartz (3), a fragment of the rhyolite (4), and a remnant of plagioclase attached to the margin of the augite grain (5). Some of the dark, fuzzy bodies in the rhyolite are thought to be sedimentary rock fragments. (b) A vesicle in the rhyolite containing a brown glass fragment (1), augite (2), hornblende (3), quartz (4), and possible plagioclase (biaxial positive, moderate 2V) grain (5). Grain 6 just outside the vesicle is probably an alkali feldspar (biaxial negative with a 2V > 50). (c) Hornblende grain in vesicle in the rhyolite. Dendritic magnetite fringes the vesicle. (d) Typical appearance of the rhyolite glass. The opaque, equant grains are magnetite, and the opaque, elongate grains are ilmenite.

DISCUSSION

Petrogenesis

Two of the most persuasive pieces of evidence for the Nenana magnetitite deposit being a lava flow are the vesicles and small-scale columnar jointing (Figs. 3 and 5). Cooling columns are characteristic of contraction as lava solidifies. They are present in lavas of the Columbia River Basalt Group, Icelandic lavas, the Giant's Causeway, Ireland, and Devil's Post Pile National Monument in California and numerous other localities. The columnar structures in the Nenana magnetitite are unusual because of their small scale. The highly vesicular zones in the magnetitite consist of small, equant to irregular vesicular zones that grade into massive rock on the scale of a thin section, suggesting a degassing lava origin. Another point supporting an extrusive magmatic origin for the magnetitite flow is its extent. Although only isolated outcrops remain (Fig. 1), the magnetitite flow occurs over a wide area, which is inconsistent with an origin from more local replacement processes, magmatic assimilation, or hydrothermal activity.

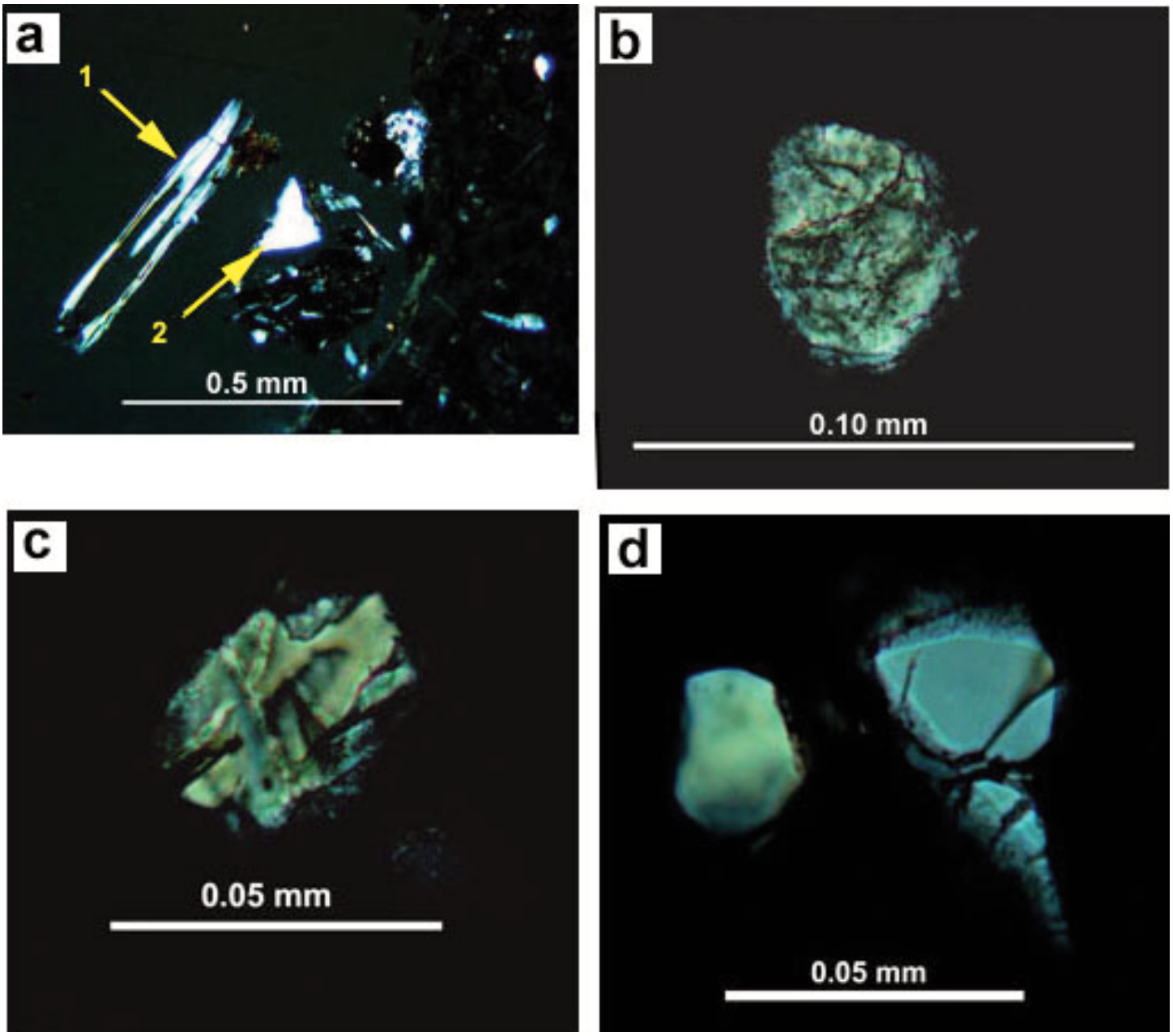

Figure 13. Photomicrographs of minerals in the rhyolite (AK-4) (all under crossed polars). (a) Muscovite (1) and plagioclase (2) in a vesicle. (b) Clinopyroxene in rhyolite glass. (c) Alkali feldspar in rhyolite glass. (d) Quartz in rhyolite glass.

We originally assumed that the magnetitite flow and the associated rhyolite had separate origins, but we now believe that their histories are intertwined. Although the magnetitite flow sits atop the rhyolite, it is clear that the magnetitite flow erupted first, and rhyolite magma was subsequently injected into the magnetitite flow along cooling joints and fractures as they were forming. However, whole rock compositions and detailed backscatter X-ray images (Fig. 17) show that the magnetitite magma also had considerable silica-rich liquid as part of it and that some of that silica-rich liquid was incorporated in magnetite as it crystallized.

We postulate that the rhyolite was injected beneath the solidified magnetitite flow as a sill-like body where it invaded the magnetitite along joints and fractures while moving or rafting all or parts of the flow. The rhyolite magma may have breached the magnetitite to form truly extrusive zones, but these cannot be demonstrated with confidence. The Dry Creek exposure has been extensively eroded by glaciation and all that remains is a remnant. All of the Usibelli Formation has been removed locally but based on the surrounding area and the California Creek exposure, Usibelli Formation sedimentary rocks were once more abundant. The California Creek expo-

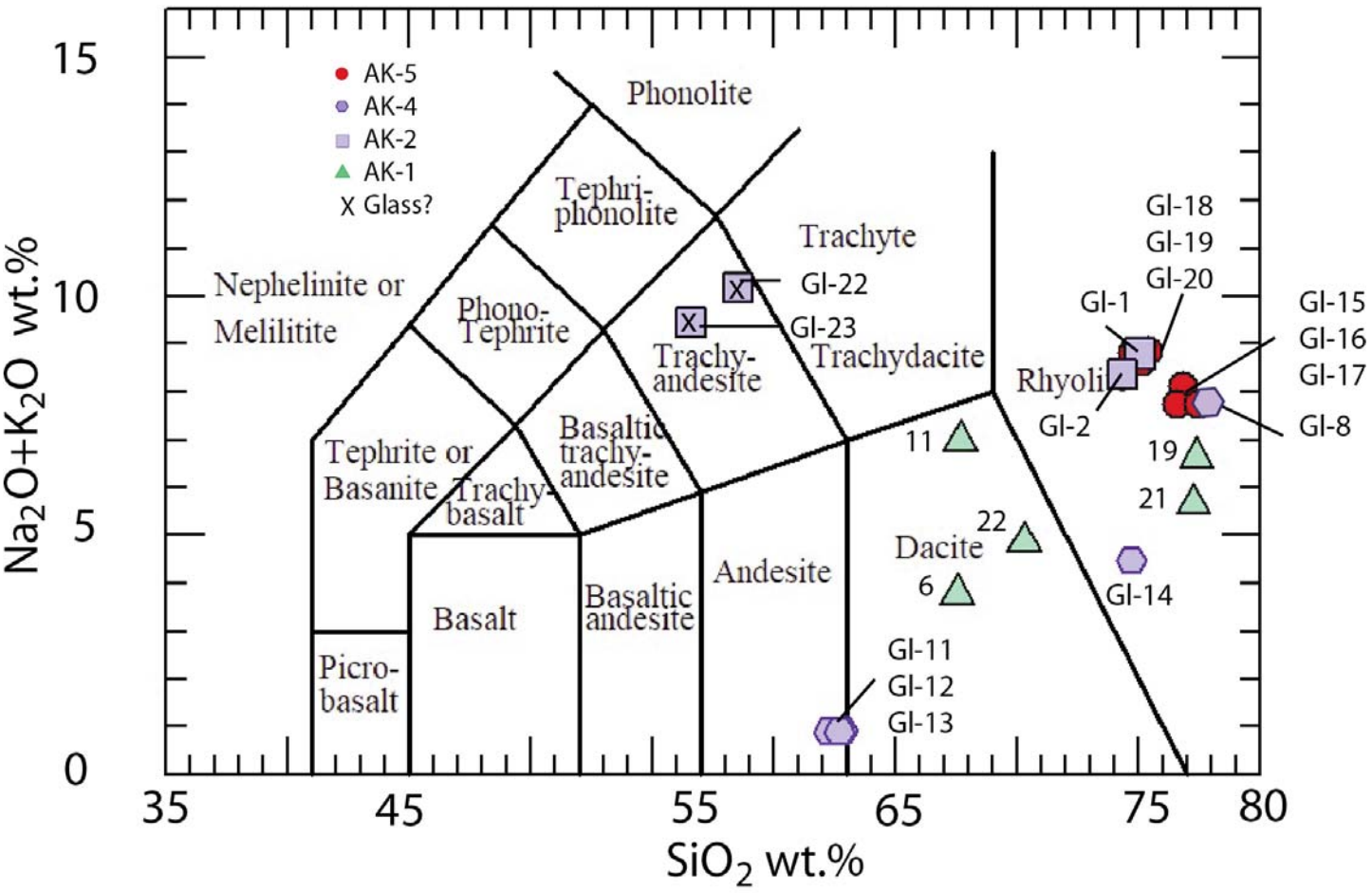

Figure 14. Diagram showing glass analyzed by microprobe for the magnetitite flow and rhyolite (AK-4). Numbers are the microprobe analysis; 'x' is for the glass analyses that might include a mineral (see text).

sure suggests that the magnetitite penetrated into unconsolidated wet sediments, but this behaviour is seen in other extrusive environments such as the Columbia River basalts (e.g. Reidel et al. 2013).

Origin of the Magnetitite Flow

Where the magnetitite flow originated is unclear. Although a possible dyke-like feeder has been identified for the rhyolite, no magnetitite dyke has been recognized and aeromagnetic anomalies provide little help due to extensive erosion.

An alternative hypothesis is that the magnetitite flow is not truly magmatic in origin, but resulted from an ancient coal-seam fire. The Nenana basin is a coal basin and coal-seam fires are known to have occurred (Wahrhaftig 1951). We can reject this hypothesis, however, by comparing the magnetitite flow to the nearby Mystic Creek coal-seam fire-induced paralava described by Reidel and Ross (in press). The Mystic Creek paralava superficially resembles a lava flow but its mode of occurrence, the presence of the unusual mineral sekaninaite, and its andesitic composition argue against such an interpretation for the Nenana magnetitite. The coal-seam fire interpretation is also inconsistent with the relationships of the Nenana magnetitite to the Usibelli Group sedimentary rocks at California Creek, and also inconsistent with the magnetitite-rhyolite relationships at the Dry Creek locality.

Our preferred hypothesis is that the magnetitite flow erupted through the same conduit as the associated rhyolite, but prior to emplacement and/or eruption of the rhyolite. Keller et al. (2022) proposed a genetic magmatic model for the El Laco magnetite–apatite deposit in Chile which bears many similarities to the Nenana magnetitite flow. The Keller et al. (2022) model is based on iron-rich (iron- oxide?) melt being derived from liquid immiscibility developed within an iron-enriched silicate magma. Although the Nenana magnetitite flow does not have the significant amount of apatite common in many other magnetitite deposits, apatite is present as microscopic grains and phosphorus comprises about 0.1 wt.% of the flow. More importantly, the physical features of the Nenana magnetitite and El Laco are similar. They resemble a basalt flow with small columns and vesicles embedded in the magnetite. One key difference between El Laco and Nenana magnetitite is that El Laco is associated with an andesite whereas the Nenana flow is closely associated with rhyolite flow. However, other magnetitite flows are associated with rhyolite (e.g. Cerro de Mercado, Lakeh Siah) so this is not unknown.

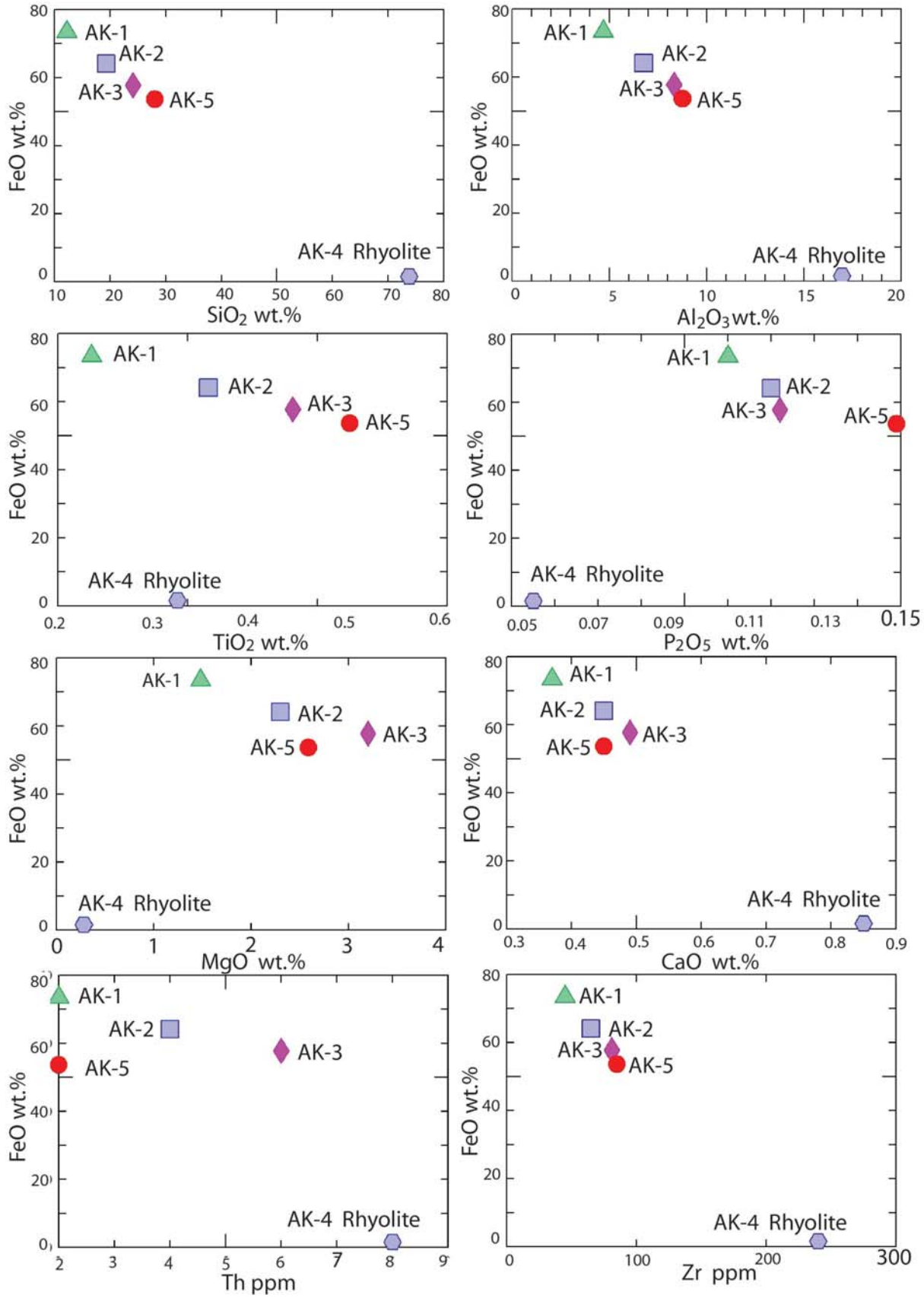

Figure 15. Geochemical variation diagrams for samples from the magnetitite flow and rhyolite (AK-4).

https://doi.org/10.12789/geocanj.2023.50.197

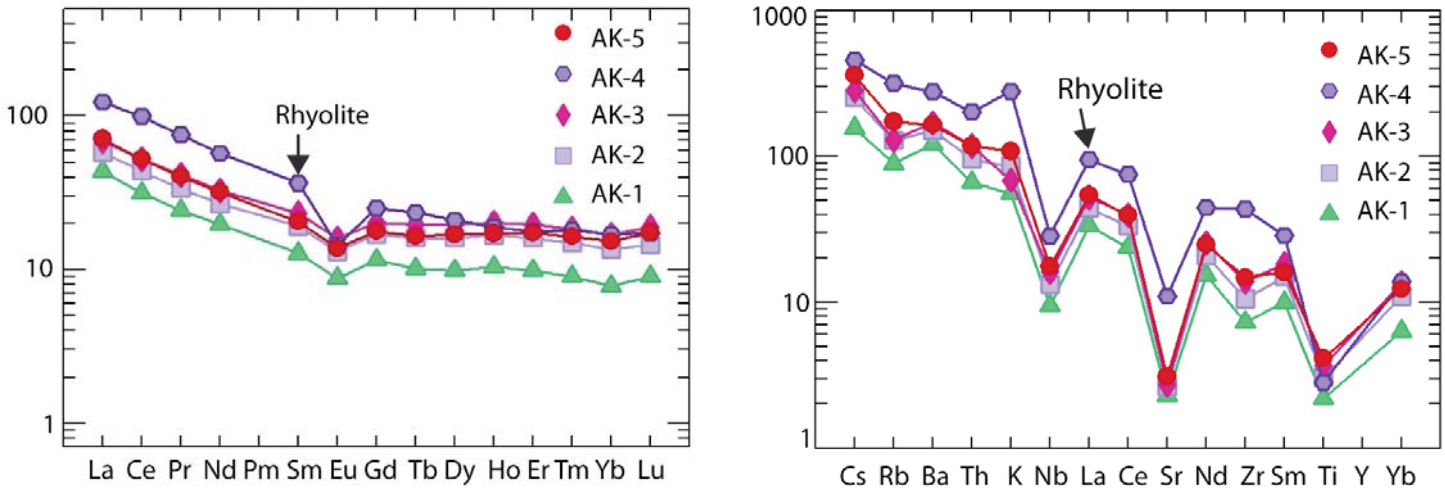

Figure 16. Trace element patterns from the magnetitite flow and rhyolite, Nenana basin, Alaska. (a) Rare earth element profiles normalized to chondrites following Sun and McDonough (1989). (b) Trace element patterns normalized to the Bulk Earth of Hickey et al. (1986).

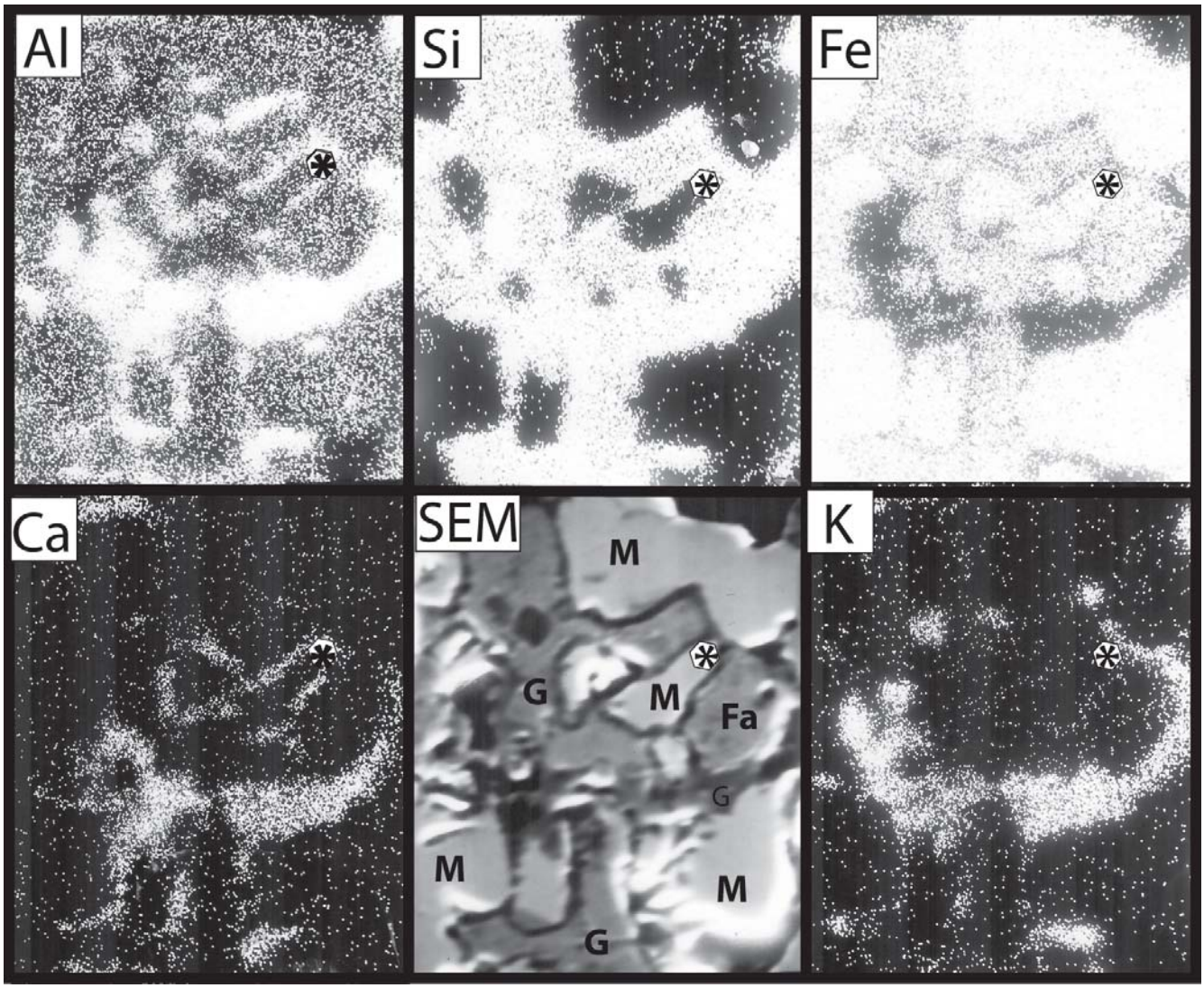

Figure 17. Scanning electron microscope (SEM) image and backscatter X-ray images from a magnetite grain in sample AK-1. Backscatter images are of the same area as in the SEM image. Magnification is 2000x. Al, aluminum; Ca, calcium; Fa, fayalite olivine; Fe, iron; G, glass; K, potassium; M-Magnetite; Si, silicon. *- reference point for each image.

The Keller et al. (2022) model envisages the 'unmixing' of andesite parent magma into a Fe-rich melt and Si-rich melt, followed by vapour-driven ascent of the magmas to the surface. With cooling, the silica-rich magma tends toward a dacite–rhyolite melt and the Fe-rich magma to magnetitite. Once the Fe-rich melt forms, it develops as micro-droplets which collect at the bottom of the magma chamber on a very short time scale. The model suggests that once the Fe-rich melt collects in this way, fracturing of rock caused by either an inflating magma chamber and/or tectonic extension provides pathways to the surface. Due to the very large contrast between the viscosity of the silica-rich melt and the Fe-rich melt (~ 6 orders of magnitude), the Fe-rich melt will ascend much faster than the silica-rich melt. However, the Fe-rich magma is unlikely to continue to ascend at the initial rate. If the volatile solubility decreases upon decompression in silica magmas, the model predicts that a magmatic volatile phase exsolves into bubbles as the Fe-rich liquid ascends. Crystallization of magnetitite upon cooling may further facilitate volatile saturation and exsolution. The volume expansion caused by this will move the liquid with an increasing speed and allow it to erupt as a lava flow.

Observations of the Nenana magnetitite flow appear to support a model like that proposed by Keller et al. (2022). The temporal relationships in which formation of the magnetitite flow eruption is followed by arrival of the rhyolite fit the Keller et al. (2022) model. The high silica content of the magnetitite flow along with the finely disseminated silica glass, silicate minerals and trace elements in magnetite grains suggest that they are remnants of an unmixing process of the same magma. Vesicles in the magnetite of the Nenana magnetitite flow indicate exsolving of volatiles into bubbles as the Fe-rich liquid ascended as proposed by Keller et al. (2022). The highly vesicular nature of the associated rhyolite also supports a vapour-driven eruption.

CONCLUSIONS

Although magnetitite flows studied from around the world are controversial, the Nenana magnetitite flow is of extrusive volcanic origin. Data supporting this interpretation include the following.

1. The extent of the magnetitite flow. Although only isolated outcrops remain in the heavily glaciated Alaska Range, the magnetitite flow occurs over a wide area suggesting that it originated as a sheet-like lava. Although localities like El Laco have multiple dykes that fed multiple localities, the Nenana magnetitite flow exposures lack obvious feeder dykes. However, one possible rhyolite feeder dyke occurs near the Dry Creek site and might also have facilitated eruption of the earlier magnetitite.
2. The high silica content of the magnetitite samples and presence of finely disseminated silica glass and minerals in the magnetite appear to be records of the magma unmixing process. This is further supported by trace element patterns (e.g. REE, trace element profiles) of the magnetitite flow and the associated rhyolite, which indicate a close relationship.
3. The magnetitite flow has vesicles and small-scale columnar jointing typical of a mafic lava flow. The highly vesicular zones in the magnetitite consist of vesicular zones that grade into massive rock on the scale of a thin section, suggesting a lava that degassed upon eruption.
4. Fractures and vesicles within the magnetitite flow contain glass and minerals typical of the associated rhyolite suggesting that the rhyolite magma invaded the magnetitite flow as a sill after the magnetitite flow had cooled and solidified. This is consistent with the timing relationships suggested by Keller et al. (2022) for the El Laco flow in Chile.

ACKNLOWLEDGEMENTS

We thank three anonymous reviewers for their review and comments that greatly improved the manuscript. In addition, we thank Andrew Kerr, Cindy Murphy and Robert Raeside for comments on the final draft that improved it and helped tie the manuscript together. We also thank B. Schoene and the Princeton University TIMS Lab for supporting our geochronology efforts. This material is based upon work funded by the National Science Foundation under Award No. 1952753.

Dr. Rick Conrey at the Peter Hooper GeoAnalytical lab at WSU provided XRF analyses. Dr. James Eckert at the Earth Materials Characterization Lab, Yale University, provided microprobe analyses of samples AK-2, AK-3, AK-4 and AK-5. B. Strope at the Rockwell International Electron Microprobe Laboratory, Richland, Washington, analyzed sample AK-1 and contributed the SEM work.

REFERENCES

Alaska Division of Geological and Geophysical Surveys, 1973a, Aeromagnetic survey, east Alaska Range, Fairbanks Quadrangle, Alaska, scale 1:250,000,1 sheet.

Alaska Division of Geological and Geophysical Surveys, 1973b, Aeromagnetic survey, east Alaska Range, Healy Quadrangle, Alaska, scale 1:250,000, 1 sheet.

Albanese, M.D., 1980, The geology of three extrusive bodies in the central Alaska Range: Unpublished MSc thesis, University of Alaska Fairbanks, 104 p., http://hdl.handle.net/11122/5943.

Athey, J.E., Newberry, R.J., Werdon, M.B., Freeman, L.K., Smith, R.L., and Szimugala, D.J., 2006, Bedrock geological map of the Liberty Bell area, Fairbanks A-4 Quadrangle, Bonnifield Mining District, Alaska: Alaska Division of Geological and Geophysical Surveys Report of Investigation 2006-2, scale 1:50,000, 98 p.

Bain, W.M., Steele-MacInnis, M., Tornos, F., Hanchar, J.M., Creaser, E.C., and Pietruszka, D.K., 2021, Evidence for iron-rich sulfate melt during magnetite (-apatite) mineralization at El Laco, Chile: Geology, v. 49, p. 1044–1048, https://doi.org/10.1130/G48861.1.

Beikman, H.M., *compiler*, 1974, Preliminary geologic map of the southeast quadrant of Alaska: U.S. Geological Survey Miscellaneous Field Studies Map 612, 2 sheets, scale 1:1,000,000.

Bowring, J.F., McLean, N.M., and Bowring, S.A., 2011, Engineering cyber infrastructure for U–Pb geochronology: Tripoli and U–Pb_Redux: Geochemistry, Geophysics, Geosystems, v. 12, Q0AA19, https://doi.org/10.1029/2010GC003479.

Condon, D.J., Schoene, B., McLean, N.M., Bowring, S.A., and Parrish, R.R., 2015, Metrology and traceability of U–Pb isotope dilution geochronology (EARTHTIME Tracer Calibration Part I): Geochimica et Cosmochimica Acta, v. 164, p. 464–480, https://doi.org/10.1016/j.gca.2015.05.026.

Dare, S.A.S., Barnes, S.-J., and Beaudoin, G., 2015, Did the massive magnetite "lava flows" of El Laco (Chile) form by magmatic or hydrothermal processes? New

constraints from magnetite composition by LA-ICP-MS: Mineralium Deposita, v. 50, p. 607–617, https://doi.org/10.1007/s00126-014-0560-1.

Dusel-Bacon, C., Aleinikoff, J.N., Premo, W.R., Paradis, S., and Lohr-Schmidt, I., 2007, Tectonic setting and metallogenesis of volcanogenic massive sulfide deposits in the Bonnifield Mining District, Northern Alaska Range, *in* Gough, L.P., and Day, W.C., *eds.*, Recent U.S. Geological Survey Studies in the Tintina Gold Province, Alaska, United States, and Yukon, Canada—Results of a 5-Year Project: U.S. Geological Survey Scientific Investigations Report 2007–5289-B, p. B1–B7, https://doi.org/10.3133/sir20075289B.

Freeman, L.K., Newberry, R.J., Werdon, M.B., Szumigala, D.J., Andrew, J.E., and Athey, J.E., 2016, Preliminary bedrock geologic map data for the eastern Bonnifield mining district, Fairbanks and Healy quadrangles, Alaska: Alaska Division of Geological and Geophysical Surveys Preliminary Interpretive Report 2016-3, 6 p., https://doi.org/10.14509/29661.

Frietsch, R., 1978, On the magmatic origin of iron ores of the Kiruna type: Economic Geology, v. 73, p. 478–485, https://doi.org/10.2113/gsecongeo.73.4.478.

Gerstenberger, H., and Haase, G., 1997, A highly effective emitter substance for mass spectrometric Pb isotope ratio determinations: Chemical Geology, v. 136, p. 309–312, https://doi.org/10.1016/S0009-2541(96)00033-2.

Gholipoor, M., Barati, M., Tale Fazel, E., and Hurai, V., 2023, Textural and compositional constraints on the origin, thermal history, and REE mobility in the Lakeh Siah iron oxide-apatite deposit—NE Bafq, Iran: Mineralium Deposita, v. 58, p. 963–986, https://doi.org/10.1007/s00126-023-01163-1.

Henriquez, F., Naslund, H.R., Nyström, J.O., Vivallo, W., Aguirre, R., Dobbs, F.M., and Lledó, H., 2003, New field evidence bearing on the origin of the El Laco magnetite deposit, northern Chile - A Discussion: Economic Geology, v. 98, p. 1497–1500, https://doi.org/10.2113/gsecongeo.98.7.1497.

Hickey, R.L., Frey, F.A., Gerlach, D.C., and Lopez-Escobar, L., 1986, Multiple sources for basaltic arc rocks from the southern volcanic zone of the Andes (34°–41°S): Trace element and isotopic evidence for contributions from subducted oceanic crust, mantle, and continental crust: Journal of Geophysical Research, v. 91, p. 5963–5983, https://doi.org/10.1029/JB091iB06p05963.

Holmes, A., 1928, The Nomenclature of Petrology, second edition: Thomas Murby and Co., London, 248 p.

Jaffey, A.H., Flynn, K.F., Glendenin, L.E., Bentley, W.C., and Essling, A.M., 1971, Precision measurement of half-lives and specific activities of ^{235}U and ^{238}U: Physical Review C, v. 4, p. 1889–1906, https://doi.org/10.1103/PhysRevC.4.1889.

Johannsen, A., 1931–1938, A Descriptive Petrology of Igneous Rocks, Volumes 1–4: University of Chicago Press.

Johnson, D.M., Hooper, P.R., and Conrey, R.M., 1999, XRF Analysis of rocks and minerals for major and trace elements on a single low dilution Li-tetraborate fused bead: Advances in X-Ray Analysis, v. 41, p. 843–867.

Kasbohm, J., and Schoene, K., 2018, Rapid eruption of the Columbia River flood basalt and correlation with the mid-Miocene climate optimum: Science Advances, v. 4, eaat8223, https://doi.org/10.1126/sciadv.aat8223.

Keller, T., Tornos, F., Hanchar, J.M., Pietruszka, D.K., Soldati, A., Dingwell, D.B., and Suckale, J., 2022, Genetic model of the El Laco magnetite-apatite deposits by extrusion of iron-rich melt: Nature Communications, v. 13, 6114, https://doi.org/10.1038/s41467-022-33302-z.

Kirschner, C.E., 1994, Interior basins of Alaska, *in* Plafker, G., and Berg, H.C., *eds.*, The Geology of Alaska, The Geology of North America, Decade of North American Geology: Geological Society of America, v. G-1, p. 469–493, https://doi.org/10.1130/DNAG-GNA-G1.469.

Krogh, T.E., 1973, A low-contamination method for hydrothermal decomposition of zircon and extraction of U and Pb for isotopic age determinations: Geochimica et Cosmochimica Acta, v. 37, p. 485–494, https://doi.org/10.1016/0016-7037(73)90213-5.

Leopold, E.B., and Liu, G., 1994, A long pollen sequence of Neogene age, Alaska Range: Quaternary International, v. 22–23, p. 103–140, https://doi.org/10.1016/1040-6182(94)90009-4.

Lyons, J.I.,1988, Volcanogenic iron oxide deposits, Cerro de Mercado and vicinity, Durango: Economic Geology, v. 83, p. 1886–1906, https://doi.org/10.2113/gsecongeo.83.8.1886.

Mattinson, J.M., 2005, Zircon U–Pb chemical abrasion ("CA-TIMS") method: Combined annealing and multi-step partial dissolution analysis for improved precision and accuracy of zircon ages: Chemical Geology, v. 220, p. 47–66, https://doi.org/10.1016/j.chemgeo.2005.03.011.

McLean, N.M., Bowring, J.F., and Bowring, S.A., 2011, An algorithm for U–Pb isotope dilution data reduction and uncertainty propagation: Geochemistry, Geophysics, Geosystems, v. 12, Q0AA18, https://doi.org/10.1029/2010GC003478.

McLean, N.M., Condon, D.J., Schoene, B., and Bowring, S.A., 2015, Evaluating uncertainties in the calibration of isotopic reference materials and multi-element isotopic tracers (EARTHTIME Tracer Calibration Part II): Geochimica et Cosmochimica Acta, v. 164, p. 481–501, https://doi.org/10.1016/j.gca.2015.02.040.

Miller, J.S., Matzel, J.E.P., Miller, C.F., Burgess, S.D., and Miller, R.B., 2007, Zircon growth and recycling during the assembly of large, composite arc plutons: Journal of Volcanology and Geothermal Research, v. 167, p. 282–299, https://doi.org/10.1016/j.jvolgeores.2007.04.019.

Naslund, H.R., Henriquez, F., Nyström, J.O., Vivallo, W., and Dobbs, F.M., 2002, Magmatic iron ores and associated mineralisation: Examples from the Chilean High Andes and Coastal Cordillera, *in* Porter, T.M., *ed.*, Hydrothermal iron oxide copper-gold and related deposits: A global perspective: Porter Geoscience Consultancy Publishing, Adelaide, v. 2, p. 207–226.

Nier, A.O., 1950, A redetermination of the relative abundances of the isotopes of carbon, nitrogen, oxygen, argon, and potassium: Physical Review, v. 77, p. 789–793, https://doi.org/10.1103/PhysRev.77.789.

Parak, T., 1985, Phosphorus in different types of ore sulfides in the iron deposits, and the type and origin of ores at Kiruna: Economic Geology, v. 80, p. 646–665, https://doi.org/10.2113/gsecongeo.80.3.646.

Park, C.F., 1961, A magnetite "flow" in northern Chile: Economic Geology, v. 56, p. 431–441, https://doi.org/10.2113/gsecongeo.56.2.431.

Péwé, T.L., Wahrhaftig, C., and Webber, F., 1966, Geologic map of the Fairbanks quadrangle, Alaska: U.S. Geological Survey Miscellaneous Geologic Investigations Map 455, scale 1:250,000.

Pietruszka, D.K., Hanchar, J.M., Tornos, F., Whitehouse, M.J., and Velasco, F., 2023, Tracking isotopic sources of immiscible melts at the enigmatic magnetite-(apatite) deposit at El Laco, Chile, using Pb isotopes: Geological Society of America Bulletin, https://doi.org/10.1130/B36506.1.

Reidel, S.P., 1984, An iron-rich lava flow from the Nenana coal field, central Alaska: *in* Short Notes on Alaskan Geology 1982–1983: Alaska Division of Geology and Geophysical Surveys, Professional Report 86B, p. 5–8, https://doi.org/10.14509/2261.

Reidel, S.P., and Ross, M.E., *in press*, A rare sekaninaite occurrence in the Nenana Coal Basin, Alaska Range, Alaska: American Mineralogist, https://doi.org/10.2138/am-2022-8698.

Reidel, S.P., Camp, V.E., Tolan, T.L., and Martin, B.S., 2013, The Columbia River flood basalt province, Stratigraphy, areal extent, volume, and physical volcanology, *in* Reidel, S.P., Camp, V.E., Ross, M.E., Wolff, J.A., Martin, B.S., Tolan, T.L, and Wells, R.E., *eds.*, The Columbia River Flood Basalt Province: Geological Society of America Special Papers, v. 497, p. 1–43, https://doi.org/10.1130/2013.2497(01).

Ross, M.E., 1989, Stratigraphic relationships of subaerial, invasive, and intracanyon flows of Saddle Mountains Basalt in the Troy basin, Oregon and Washington, *in* Reidel, S.P., and Hooper, P.R., *eds.*, Volcanism and Tectonism in the Columbia River Flood-Basalt Province: Geological Society of America Special Papers, v. 237, p. 131–142, https://doi.org/10.1130/SPE239-p131.

Sillitoe, R.H., and Burrows, D.B., 2002, New field evidence bearing on the origin of the El Laco magnetite deposit, northern Chile: Economic Geology, v. 97, p. 1101–1109, https://doi.org/10.2113/gsecongeo.97.5.1101.

Sillitoe, R.H., and Burrows, D.B., 2003, New field evidence bearing on the origin of the El Laco magnetite deposit, northern Chile - A Reply: Economic Geology, v. 98, p. 1501–1502, https://doi.org/10.2113/gsecongeo.98.7.1501.

Simon, J.I., Renne, P.R., and Mundil, R., 2008, Implications of pre-eruptive magmatic histories of zircons for U–Pb geochronology of silicic extrusions: Earth and Planetary Science Letters, v. 266, p. 182–194, https://doi.org/10.1016/j.epsl.2007.11.014.

Sortor, R.N., Goehring, B.M., Bemis, S.P., Ruleman, C.A., Caffee, M.W., and Ward, D.J., 2021, Early Pleistocene climate-induced erosion of the Alaska Range formed the Nenana Gravel: Geology, v. 49, p. 1473–1477, https://doi.org/10.1130/G49094.1.

Sun, S.-s., and McDonough, W.F., 1989, Chemical and isotopic systematics of oceanic basalts: Implications for mantle composition and processes, *in* Saunders, A.D., and Norry, M.J., *eds.*, Magmatism in the Ocean Basins: Geological Society Special Publications, v. 42, p. 313–345, https://doi.org/10.1144/GSL.SP.1989.042.01.19.

Triplehorn, D.M., Drake, J., and Layer, P.W., 2000, Preliminary $^{40}Ar/^{39}Ar$ ages from two units in the Usibelli Group, Healy, Alaska: New light on some old problems, *in* Pinney, D.S., and Davis, P.K., *eds.,* Short Notes on Alaska Geology 1999: Alaska Division of Geological and Geophysical Surveys Professional Report 119I, p. 117–127, https://doi.org/10.14509/2691.

Wahrhaftig, C., 1951, Geology and coal deposits of the western part of the Nenana coal field, Alaska, *in* Barnes, F.F., *ed.*, Coal investigations in south-central Alaska,

1944–46: U.S. Geological Survey Bulletin 963-E, p. 169–186.
Wahrhaftig, C., 1970a, Geologic map of the Healy D-2 quadrangle, Alaska: U.S. Geological Survey Geologic Quadrangle Map GQ-804, scale 1:63,360, 1 sheet.
Wahrhaftig, C.,1970b, Geologic map of the Healy D-3 quadrangle, Alaska: U.S. Geological Survey Geologic Quadrangle Map GQ-805, scale 1:63,360, 1 sheet.
Wahrhaftig, C., 1970c, Geologic map of the Healy D-4 quadrangle, Alaska: U.S. Geological Survey Geologic Quadrangle Map GQ-806, scale 1:63,360, 1 sheet.
Wahrhaftig, C., 1970d, Geologic map of the Healy D-5quadrangle, Alaska: U.S. Geological Survey Geologic Quadrangle Map GQ-807, scale 1:63,360, 1 sheet.
Wahrhaftig, C., 1970e, Geologic map of the Fairbanks A-2 quadrangle, Alaska: U.S. Geological Survey Geologic Quadrangle Map GQ-808, scale 1:63,360, 1 sheet.
Wahrhaftig, C., 1970f, Geologic map of the Fairbanks A-3 quadrangle, Alaska: U.S. Geological Survey Geologic Quadrangle Map GQ-809, scale 1:63,360, 1 sheet.
Wahrhaftig, C., 1970g, Geologic Map of the Fairbanks A-4 Quadrangle, Alaska: U.S. Geological Survey Geologic Quadrangle Map 810, scale 1:63,360, 1 sheet, https://dggs.alaska.gov/webpubs/usgs/gq/oversized/gq-0810sht01.pdf.
Wahrhaftig, C., 1970h, Geologic map of the Fairbanks A-5 quadrangle, Alaska: U.S. Geological Survey Geologic Quadrangle Map GQ-811, scale 1:63,360, 1 sheet.
Wahrhaftig, C., 1987, The Cenozoic section at Suntrana, Alaska, *in* Hill, M.L., *ed.*, Cordilleran Section of the Geological Society of America: Geological Society of America, The Decade of North American Geology (DNAG), Centennial Field Guide 1, p. 445–450, https://doi.org/10.1130/0-8137-5401-1.445.
Wahrhaftig, C., Wolfe, J.A., Leopold, E.B., and Lanphere, M.A., 1969, The coal-bearing group in the Nenana coal field, Alaska: Contributions to Stratigraphy: U.S. Geological Survey Bulletin 1274-D, p. D1–D30, https://doi.org/10.3133/b1274D.
Wartes, M.A, Gillis, R.J., Herriott, T.M., Stanley, R.G., Helmold, K.P., Peterson, C.S., and Benowitz, J.A., 2013, Summary of the 2012 reconnaissance field studies related to petroleum geology of the Nenana basin, interior Alaska: Division of Geological and Geophysical Surveys, Alaska Geological Survey, Preliminary Interpretive Report 2013-2, 13 p., https://doi.org/10.14509/24880.
Wilson, F.H., Dover, J.H., Bradley, D.C., Weber, F.R., Bundtzen, T.K., and Haeussler, P.J., 1998, Geologic map of central (interior) Alaska: U.S. Geological Survey Open-File Report OF 98-133-A, version 1.2, https://pubs.usgs.gov/of/1998/of98-133-a/.
Wolfe, J.A., and Tanai, T., 1987, Systematics, phylogeny, and distribution of Acer (Maples) in the Cenozoic of western North America: Journal of the Faculty of Science, Hokkaido University, v. 22, p. 1–246, http://hdl.handle.net/2115/36747.

Received February 2023
Accepted as revised April 2023

For access to the Reidel et al. (2023) Supplementary Material, Appendix A: Petrographic Data, Appendix B: Microprobe Analyses, Appendix C: Chemical Analyses, and Appendix D: U–Pb Geochronological Data, please visit the GAC's open source GC Data Repository for the Igneous Rock Associations Series at: https://gac.ca/gc-data-repository/.

GEOLOGICAL ASSOCIATION OF CANADA
(2023–2024)

Corporate Members

PLATINUM

MEMORIAL UNIVERSITY

GOLD

AngloAmerican

NORTHWEST TERRITORIES GEOLOGICAL SURVEY

SILVER

ROYAL TYRRELL MUSEUM

YUKON GEOLOGICAL SURVEY

BRITISH COLUMBIA GEOLOGICAL SURVEY

NICKEL

UNIVERSITY OF WATERLOO — CONCORDIA CUM VERITATE

GEOSCIENCE CANADA AND THE GEOLOGICAL ASSOCIATION OF CANADA ARE GRATEFUL TO THE CANADIAN GEOLOGICAL FOUNDATION FOR THEIR FINANCIAL SUPPORT OF THIS JOURNAL

Canadian Geological Foundation — Fondation Géologique du Canada — 1968

Officers

President
Alwynne Beaudoin
Vice-President
Nikole Bingham-Koslowski
Treasurer
Deanne van Rooyen
Secretary
Tim Fedak

Councillors

Alwynne Beaudoin
Nikole Bingham-Koslowski
Kirstin Brink
Tim Fedak
David Lowe
Nadia Mohammadi
David Moynihan
Deanne van Rooyen
Rajeev Sasidharan Nair
Ricardo Silva
Diane Skipton
Colin Sproat

GAC Editors

GAC Books
Vacant
Geolog
Roger Paulen
Geoscience Canada
Andy Kerr

Standing Committees

Communications
Kirstin Brink
Finance
Deanne van Rooyen
GAC Lecture Tours
Nadia Mohammadi
Publications
David Lowe
Science Program
Rajeev Sasidharan Nair